2015

Identification of Candidate Genes for Craniosynostosis

Karen Rymer
Virginia Commonwealth University

Identification of Candidate Genes for Craniosynostosis

Karen Suzanne Rymer

VIRGINIA COMMONWEALTH UNIVERSITY
DEPARTMENT OF HUMAN AND MOLECULAR GENETICS
2015

IDENTIFICATION OF CANDIDATE GENES FOR CRANIOSYNOSTOSIS

A thesis submitted in partial fulfillment of the requirements for the degree of Master of Science at Virginia Commonwealth University

By

Karen Suzanne Rymer
Bachelor of Science, Mathematics, Liberty University, 2013
Bachelor of Science, Biology: Premed, Liberty University, 2013

Director: RITA SHIANG, Ph.D.
ASSOCIATE PROFESSOR
DEPARTMENT OF HUMAN AND MOLECULAR GENETICS

Virginia Commonwealth University
Richmond, VA
April, 2015

Acknowledgement

I would first like to thank Dr. Rita Shiang, who has guided me through this (seemingly endless) journey towards my master's degree. I could not have come this far without her advice, constructive criticism, and extreme patience. Dr. Shiang has made my days in lab educational, yet very enjoyable.

I would also like to thank my committee members for the part they all played to make this project a reality. Dr. Jennifer Rhodes made this project possible through her work in the Center for Craniofacial Care at Virginia Commonwealth University. Dr. Jim Lister's expertise in the zebrafish model system has provided endless help for my animal model testing. Dr. Todd Webb was able to handle all of my bioinformatics and coding questions with ease.

I cannot forget my lab members Anting, Laura, and Danielle. I could not have survived early mornings or late nights without the constant supply of caffeine and food that was provided (of course no food was eaten in lab).

Last, but certainly not least, I would like to thank my husband, Alex, and my mom and dad for always being there for me. They have supported me through my most stressful times, as well as celebrated with me in my triumphs. No matter what happens, I know I have the love and support of my family.

Table of Contents

List of Figures, Tables and Appendices

List of Abbreviations

ACH – Achondroplasia

Amp – ampicillin

AN – acanthosis nigricans

AR – androgen receptor

BAM – binary alignment and mapping

BAMBI – BMP and activin membrane-bound inhibitor

BLAST – basic local alignment search tool

BMP – bone morphogenic protein

BSP – bone sialoprotein

BWA – Burrows-Wheeler Alignment

CCD – cleidocranial dysplasia

CYP26B1 – cytochrome P450, family 26, subfamily B, polypeptide 1

dpf – days past fertilization

ERK – extracellular signal related kinase

FAK – focal adhesion kinase

FGF – fibroblast growth factor

FGFR – fibroblast growth factor receptor

FRAS1 – Fraser Syndrome 1 homolog

FREM1 – FRAS1 related extracellular matrix 1

GRB2 – growth factor bound 2

gRNA – guide RNA

HCH – Hypochondroplasia

HRNR – hornerin

IBD – identity by descent

Ig – immunoglobin like

IGV – Integrated Genome Viewer

ITGAV – integrin alpha V

JNK – Jun-amino terminal kinase

LB – Luria broth

MAF – minor allele frequency

MESAB – Ethyl 3-aminobenzoate, methanesulfonic acid salt

MSX2 – msh homeobox 2

NEB – New England Biolabs

NF-κB –nuclear factor B

NSC – nonsyndromic craniosynostosis

PAK – p21 activated kinase

PBD – Protein Data Bank

RUNX2 – runt-related transcription factor 2

SAM – standard alignment and mapping

SAP – shrimp alkaline phosphatase

SLC30A9 – solute carrier family 30, member 9

SOS – son of sevenless

TD – Thanatophoric dysplasia

TWIST1 – twist family bHLH transcription factor 1

vcf – variant call format

WES – whole exome sequencing

WGS – whole genome sequencing

Abstract

IDENTIFICATION OF CANDIDATE GENES FOR CRANIOSYNOSTOSIS

By Karen Suzanne Rymer

A thesis submitted in partial fulfillment of the requirements for the degree of
Master of Science at Virginia commonwealth University

Virginia Commonwealth University, 2015

Major Director: Dr. Rita Shiang
Associate Professor, Department of Human and Molecular Genetics

Craniosynostosis is a disorder characterized by the premature fusing of cranial sutures in an infant. Premature closure of these sutures can lead to detrimental consequences on the development of a child. The two broad categories of craniosynostosis are classified as syndromic and nonsyndromic. Nonsyndromic craniosynostosis involves only the fusion of one or more sutures, whereas syndromic craniosynostosis involves other abnormalities throughout the body of the affected individual. Two of the families analyzed in this study were of the syndromic nature, and known FGFR mutations were discovered. However, phenotypical features documented in association with these mutations differed from our individuals. Two families affected with nonsyndromic sagittal synostosis were also analyzed. Within one of these families, three candidate mutations were identified as possible disease causing mutations. These mutations were found in the genes ITGAV, SLC30A9, and BAMBI. Here we analyze the function of these proteins and determine the significance of the role they may play in nonsyndromic craniosynostosis.

Chapter 1: Introduction

The human brain is by far one of the most complex and intricate organs to develop during embryogenesis. Without the sophisticated neural networks of the brain, the cells of the body have no control center. Anything preventing or hindering the development of the brain can have detrimental effects on the developing fetus, and can often lead to fatality. Craniosynostosis is one of the many disorders that affect the development of the brain by preventing proper growth. Craniosynostosis is defined as "a birth defect that causes one or more of the sutures on an infant's skull to close earlier than usual." (Kinsman et al. 2011). Premature closing of these sutures can lead to abnormal development caused by the inability of the bones to move and expand in accordance with the growth of the brain.

Cranial Bone Development

Human skull bones begin to develop during 23-26 days of gestation. Formation of the cranial bones occurs via intramembranous ossification, a process that lacks the cartilage intermediate that is found within most of the bones of the body (Beederman, et al. 2014). Intramembranous ossification is defined as "the direct conversion of mesenchymal tissue into bone" (Gilbert, et al. 2000). During intramembranous ossification in the skull, neural crest-derived mesenchymal cells proliferate and condense. Some of these cells become capillaries, while others differentiate into osteoblasts and begin to secrete a collagen-proteoglycan matrix. This matrix has the ability to bind calcium salts, allowing the calcification process to proceed. Bone morphogenetic proteins (BMP) from the head epidermis are thought to influence the conversion of the mesenchymal cells into osteocytes (Gilbert, et al. 2000). These mesenchymal cells are located between the dermal mesenchyme and the meninges of the brain. Areas that will eventually form the skull sutures remain undifferentiated (Beederman, et al. 2014).

One transcription factor that is crucial to the development of bones throughout the body is runt-related transcription factor 2 (RUNX2, aka CBFA1). RUNX2 is a BMP activated transcription factor that regulates the transformation of mesenchymal cells into osteoblasts. Confirmation of this role was obtained via a RUNX2 homozygous knockout study in mice (Gilbert, et al. 2000). Prior to determination of RUNX2's function, Komori et al. (1997) and Otto et al. (1997) showed that homozygous deletion of the RUNX2 gene caused fatality immediately after birth. Mice with this mutation had only cartilaginous skeletal models, thus exhibiting a complete lack of bone through elimination of both endochondral and intramembranous ossification. Heterozygous knockouts of RUNX2 showed a complete lack of skull suture fusion, as well as stunted growth and clavicle absence, a phenotype similar to cleidocranial dysplasia (CCD). This study led to the determination that CCD in humans is caused by heterozygosity of the RUNX2 gene (Mundulos, et al. 1997).

Skulls are comprised of two frontal bones, two parietal bones, two temporal bones, one sphenoid bone, and one occipital bone (Figure 1). Sutures are classified as the fibrous areas where two bones come into contact with one another. Fontanelles are the specific location where multiple sutures come into contact with each other and there is often a lack of bone in this area, thus creating a "soft spot". There are two fontanelles in the newborn skull, the anterior fontanelle and the posterior fontanelle (Figure 1) (Beederman, et al. 2014)

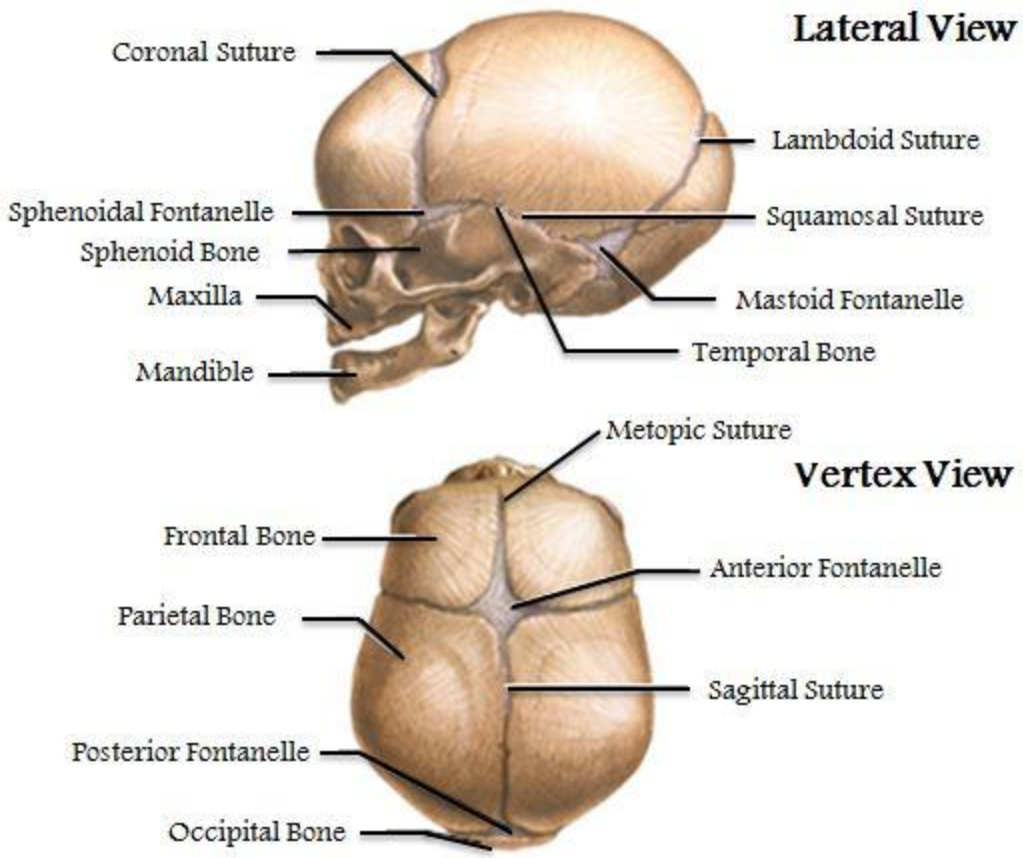

Figure 1. Anatomical drawings of a newborn skull from a lateral and vertex view. Taken and edited from http://www.nlmnih.gov/medlineplus/ency/imagepages/1127.htm

Cranial Sutures

A newborn skull contains five main sutures: metopic, lambdoid, coronal, sagittal, and squamous, as shown in Figures 1 and 2 (Carlo et al. 2011). The sagittal suture lies most superiorly on the newborn skull and is located between the two parietal bones. Two of the sutures are split into right and left sides, the coronal and lambdoid sutures. The coronal sutures are located between the two frontal and parietal bones, and the lambdoid sutures are between the supraoccipital and parietal bones. In the same line as the sagittal suture lies the metopic suture, located between the two frontal bones. Most posteriorly on the skull is the squamosal suture, located between the temporal, parietal, and sphenoid bones (Beederman, et al. 2014).

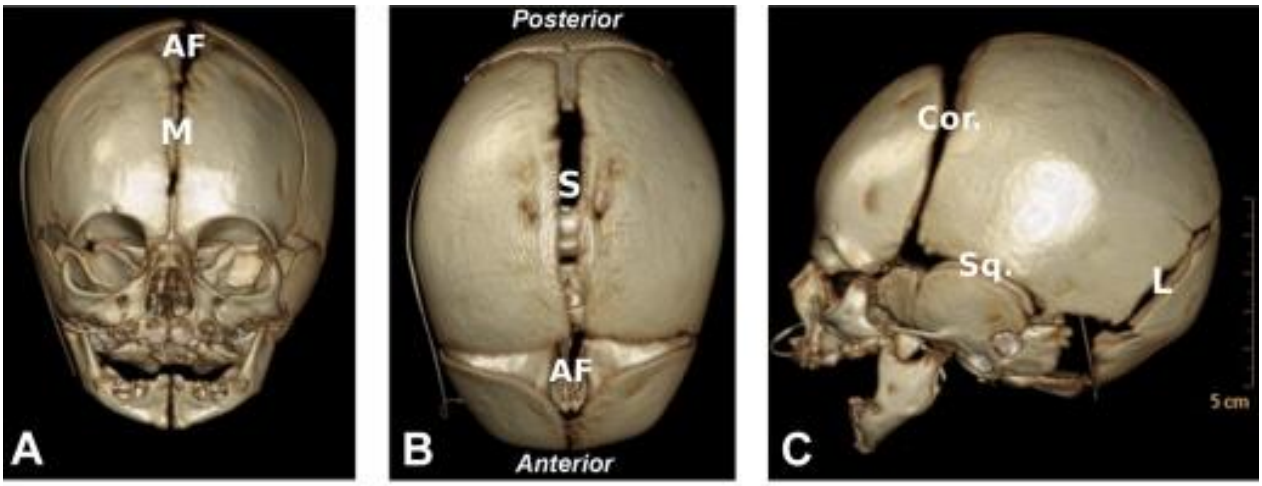

Figure 2. Three-dimensional computed tomography reconstructions of a 4-week-old patient with normal suture development (A–C). Anterior (A), vertex (B), and lateral (C) views. (A–C) Typical skull contour with patent sutures. AF, anterior fontanelle; M, metopic suture; S, sagittal suture; Cor., coronal suture; Sq., squamosal suture; L, lambdoid suture. Taken from Beederman, et al. 2014.

Sutures form in an interdigitated pattern caused by the expression of several classes of molecules. Using a mouse model, several osteoblastic proteins were localized at the osteogenic fronts and within the sutural mesenchyme of the calvarial bones (frontal, parietal, and interparietal). RUNX2, BMP (both described above), and bone sialoprotein (BSP) are three of the proteins expressed at the osteogenic fronts of the cranial bones. BSP is an extracellular matrix protein produced by osteoblasts and is thought to play a role in the process of bone mineralization. As development progresses, expression of both BSP and RUNX2 becomes more restricted to areas of high osteogenic activity, or sutural bone ends, as development progresses.

Two transcription factors thought to regulate osteogenic lineage crucial to the development of the skull are msh homeobox 2 (MSX2) and twist family bHLH transcription factor 1 (TWIST1). These two have been found to be extensively expressed in the cranial mesenchyme. Similar to BSP and RUNX2, as development progresses, TWIST1 and MSX2 expression become restricted to mid-sutural mesenchyme between the osteogenic fronts. As mesenchymal cells differentiate into mature osteoblasts, their gene expression profile changes from TWIST1 and MSX2 to FGFR2c and MSX2. All transcripts of the fibroblast growth factor receptor (FGFR) genes FGFR1, FGFR2, and FGFR3, with the exception of the FGFR1b and FGFR3b isoforms, are localized within the sutural mesenchyme. FGFRs are a family of receptor tyrosine kinases that bind fibroblast growth factors (FGF). Most notably, FGFR2c transcripts have been detected with high intensity in the sutural osteogenic fronts of the developing skull (Rice, et al. 2003).

In Rice et al. (2003) upstream mediators and downstream targets of BMPs and FGFs were evaluated through a study involving beads coated with different FGF or BMP proteins. Results showed that FGF4 upregulated expression of MSX1, BMP2 upregulated MSX2, and

BMP4 was found to upregulate both MSX1 and MSX2. FGF2 was shown to induce TWIST1 mRNA. FGF4 beads were placed on the osteogenic fronts caused accelerated sutural closure, similar to craniosynostosis phenotypes. These studies gave an indication of the signaling networks involved in suture biology.

At approximately 18 months of age, the metopic suture begins to fuse, making it the first suture to fuse in a typical infant (Morriss-Kay, et al. 2005). The last suture to fuse is the sagittal suture, a process that generally does not take place until approximately 25 years of age (Beederman, et al. 2014).

The patency of the sutures corresponds to the growth of the brain throughout the development of a child. The brain experiences a rapid growth through the first few years of the child's life, reaching approximately 70% of its final weight by 2 years of age (Huelke, et al. 1998). The brain then begins to plateau and does not reach its estimated adult size until around early adolescence (Derderian, et al. 2012). Thus, it is crucial for the sutures to remain patent to avoid increased intracranial pressure within the skull. Increased intracranial pressure can damage the brain or spinal cord by pressing on certain areas of the brain and restricting blood flow, causing a lack of oxygen to that area. This can lead to detrimental consequences on the development of the child. Some of these consequences include developmental delay, hydrocephalus, visual abnormalities, airway impairment, and orthodontic defects (Anantheswar, et al. 2009).

Syndromic Craniosynostosis

There are two broad categories of craniosynostosis: syndromic and nonsyndromic. The overall prevalence of craniosynostosis is approximately 1 in 2500 births (Johnson, et al. 2011). Syndromic craniosynostosis accounts for approximately 25% of all cases and can result from

over 180 monogenic syndromes, such as Crouzon, Apert, Pfeiffer, and Muenke syndrome (Greenwood, et al. 2014). What sets these disorders apart from nonsyndromic craniosynostosis is that the premature fusing of the skull bones occurs with other features such as exophthalmos, midface hypoplasia, uncharacteristic facies, and limb abnormalities (Derderian, et al. 2012). Ethnic prevalence within syndromic craniosynostosis patients varies depending on which syndrome the individual has.

Nonsyndromic Craniosynostosis

Nonsyndromic craniosynostosis (NSC), which is the focus of this study, occurs when the affected individual shows no other clinical features aside from the skull anomalies. No clear association has been discovered between ethnicity and NSC. Single suture forms represent a majority of the nonsyndromic cases and are classified according to which suture is fused at the birth of the child (Lattanzi, et al. 2012). Complex suture synostosis, found in approximately 5-15% of nonsyndromic cases, occurs when multiple sutures are fused (Morriss-Kay, et al. 2005). Complex synostosis phenotypes depend upon which sutures are fused. The phenotype is often a combination of the clinical features of those categories (Greenwood, et al. 2014).

Sagittal synostosis, or scaphocephaly, is the most common type of nonsyndromic craniosynostosis, with a percentage of roughly 45-50% of nonsyndromic cases. Scaphocephaly occurs in approximately 1 in 5,000 births (Greenwood, et al. 2014). This type arises in a male to female ratio of 2.5:1. Sagittal suture fusion results in a long and narrow skull, leading to the name “scapho” meaning boat in Greek. (Figure 3a)

The second most common type is coronal synostosis, or anterior plagiocephaly. Coronal synostosis can either be unicoronal or bicoronal, affecting one or both sides of the coronal suture. It is more common for coronal synostosis to be seen in the unicoronal presentation. This makes

up approximately 25-30% of NSC cases and shows female prevalence with a 1:2.3 male to female ratio (Lattanzi, et al. 2012). Anterior plagiocephaly is clinically characterized by flattening of the forehead on the affected side, often leading to an elevated eye socket or deviated nose (Garza, et al. 2012). (Figure 3b)

Metopic craniosynostosis is the premature fusion of the metopic suture and accounts for approximately 14% of NSC cases. This category has a male to female ratio of 3.3:1 (Greenwood, et al. 2014). Metopic synostosis is also known as trigonocephaly due to the triangular shape of the forehead with bifrontal and bitemporal narrowing, as well as parietal and occipital prominence (Garza, et al. 2012). (Figure 3c)

Lambdoid synostosis, the least common, is found in only 3% of NSC cases (Lattanzi, et al. 2012). Also called posterior plagiocephaly, lambdoid synostosis presents with an occipital dysmorphism involving a mastoid bulge and a thick ridge along the affected side of the lambdoid suture (Garza, et al. 2012). This phonotypical presentation is similar to the coronal synostosis, but on the posterior aspect of the child's head. (Figure 3d)

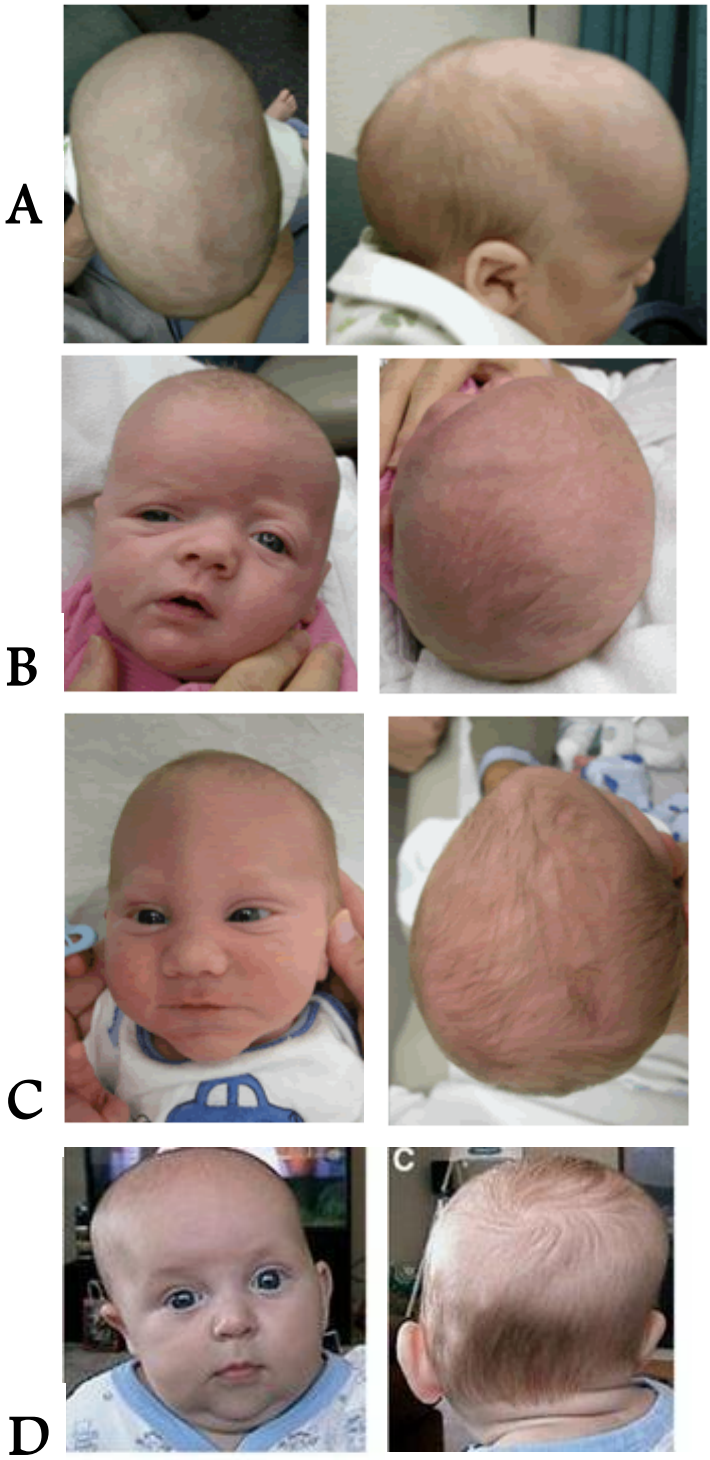

Figure 3. (A) Sagittal craniosynostosis from a vertex and lateral view. (B) Right coronal synostosis from an anterior and vertex view. (C) Metopic craniosynostosis from an anterior and vertex view. (D) Left lambdoid craniosynostosis from an anterior and posterior view. Taken from Ciurea, et al and Pincus, et al.

Treatment Options

Due to the lack of knowledge surrounding the causes of nonsyndromic craniosynostosis, prevention is not yet a possibility. The only treatment option available at this time is surgical intervention. Surgery to separate fused sutures must be performed when the affected child is still within his or her first year of life. The primary goals of surgical intervention are to relieve pressure on the brain and separate the sutures in order to allow the child's head to grow, as it should during normal development (Kinsman et al. 2011). Craniofacial surgery is a combination of neurosurgery, plastic surgery, occuloplastics, ENT, and neck specialties. (Anantheswar, et al. 2009) Proper timing of surgery is vital to the survival of the infant. The common philosophy is to perform surgery as soon as the child is able to withstand the stress (Garza, et al. 2012).

Complications involved in an open surgical repair include bleeding, infection, cerebrospinal fluid leak, failure of re-ossification, contour irregularity, meningitis, stroke, and even death. Previous research has shown that patients who underwent surgery prior to 6 months of age had a less successful outcome and often needed a second operation. Thus, the general consensus among surgeons is to perform surgery between 6 and 12 months of age. Current research is focusing on understanding the genetic basis of craniosynostosis in order to provide opportunities for earlier and more specific interventions, as well as targeted gene therapy for the prevention of premature suture fusion (Garza, et al. 2012).

Genetics of Syndromic Craniosynostosis

FGFR Genes

Although a clear genetic background for all types of nonsyndromic craniosynostosis has not been determined yet, several genes have been identified for syndromic craniosynostosis. A group of genes, the FGFRs, are known to cause a craniosynostosis phenotype. FGFRs, as

described above, bind FGFs, a family of at least 22 signaling molecules that play a regulatory role during embryonic development (Hughes, et al. 1997). FGF signaling is crucial to endochondral and intramembranous ossification (Lattanzi, et al. 2012). There are four members of the FGFR family, labeled FGFR1, FGFR2, FGFR3, and FGFR4. The binding of FGFRs to their ligand is promiscuous, meaning any receptor can bind any one of the signaling molecules. Each FGFR has a cytoplasmic tyrosine kinase domain, a transmembrane domain, and an extracellular domain consisting of three immunoglobulin (Ig)-like domains. Ligands bind between the second and third Ig-like domains, allowing the receptors to dimerize and an intracellular signaling cascade to proceed (Robin, et al. 1998).

Despite widespread tissue localization, mutations in the FGFR family primarily lead to a variety of bone abnormalities during development. As shown in Figure 4, several craniosynostosis phenotypes have been associated with three of the FGFR genes. FGFR mutations have also been identified for multiple other disorders such as achondroplasia, hypochondroplasia, Antley-Bixler syndrome, and Saethre-Chotzen. There are craniosynostosis syndromes with identified FGFR mutations, as shown in Table 1. Of the eight FGFR related craniosynostosis syndromes, six can be diagnosed by characteristic facial features, hand and foot abnormalities, and skull shape. These six are Pfeiffer syndrome, Apert syndrome, Crouzon syndrome, Beare-Stevenson syndrome, Jackson-Weiss syndrome, and Crouzon with acanthosis nigricans (AN). The other two, Muenke syndrome and FGFR2-related isolated coronal synostosis, require molecular genetic testing. Muenke syndrome may have uni- or bicoronal synostosis or megalocephaly without craniosynostosis, thus requiring an FGFR3 P250R mutation for diagnosis. This same mutation has been associated with nonsyndromic coronal

craniosynostosis. FGFR2-related isolated coronal synostosis is characterized by uni- or bicoronal craniosynostosis only (Robin, et al. 1998).

The most characterized FGFR1 mutation that has been shown to cause syndromic craniosynostosis is the Pfeiffer syndrome P252R missense mutation. As for FGFR3, the only craniosynostosis mutation identified is the A391E mutation causing Crouzon syndrome. However, individuals with only Crouzon syndrome are unlikely to have a mutation in FGFR3 (Robin, et al. 1998). All other FGFR3 mutations identified cause varying types of skeletal dysplasia. Currently, no mutations in FGFR4 have been identified to cause craniofacial disorders.

Multiple mutations in the FGFR2 gene have been identified in several different syndromic craniosynostosis disorders. Apert syndrome is caused by both the S252W and P243R mutations. Mutations within the third immunoglobulin domain have been shown to cause Crouzon, Pfeiffer, and Jackson-Weiss syndrome, as noted in Figure 4. Different mutations at the same residue (W290G, W290R, W290H, W290C) result in either Pfeiffer syndrome or Crouzon, suggesting the role of epigenetics factors, modifier genes, or control sequences (Robin, et al. 1998).

Table 1. FGFR Related Craniosynostosi Disorders

	Craniofacial	Extremities	Intellect	Skin	Other
Crouzon syndrome	Coronal synostosis Proptosis External strabismus Mandibular prognathism	Normal	Normal	Normal	Hydrocephalus Tonsillar herniation Sacrococcygeal tail
Crouzon syndrome with AN	Coronal synostosis Proptosis External strabismus Mandibular prognathism	Normal	Normal	Acanthosis nigricans	None
Apert syndrome	Turribrachycephaly Midface hypoplasia	Syndactyly Rhizomelic shortening Elbow ankyloses	Intellectual disability	Normal	Fused cervical vertebrae Cardiac defects Gastrointestinal defects Ovarian dysgerminoma
Pfeiffer Type 1	Midface hypoplasia	Broad and medially deviated thumbs and great toes Bradydactyly	Normal	Normal	Hearing loss Hydrocephalus
Pfeiffer Type 2	Cloverleaf skull Extreme proptosis	Broad and medially deviated thumbs and great toes Ankyloses of elbows and knees Bradydactyly	Intellectual disability	Normal	Choanalstenosis Laryngotracheal abnormalities Hydrocephalus Seizures Sacrococcygeal eversion Cleft palate
Pfeiffer Type 3	Turribrachycephaly Extreme proptosis	Broad and medially deviated thumbs and great toes Ankyloses of elbows and knees Bradydactyly	Intellectual disability	Normal	Choanalstenosis Laryngotracheal abnormalities Hydrocephalus Seizures
Muenke syndrome	Variable Uni or bilateral coronal Midface hypoplasia Megalocephaly Ocular hypertension	Variable Carpal-tarsal fusion Brachydactyly Carpal bone malsegregation Coned epiphyses	Normal to mild intellectual disability	Normal	Bilateral, symmetrical low to mid frequency hearing loss Osteochondroma
Jackson-Weiss	Mandibular prognathism	Broad and medially deviated great toes Short first metatarsal Calcaneocuboid fusion Abnormal tarsals	Normal	Normal	None
Beare-Stevenson	Moderate to severe midface hypoplasia Abnormal ears Natal teeth	Furrowed palms and soles	Intellectual disability	Widespread cutis gyrate Acanthosis nigricans Prominent umbilical stump	Bifid scrotum Prominent labial raphe/rugated labia majora Pyloric stenosis Anterior anus
FGFR2-related isolated coronal synostosis	Unilateral coronal synostosis	Normal	Normal	Normal	Normal

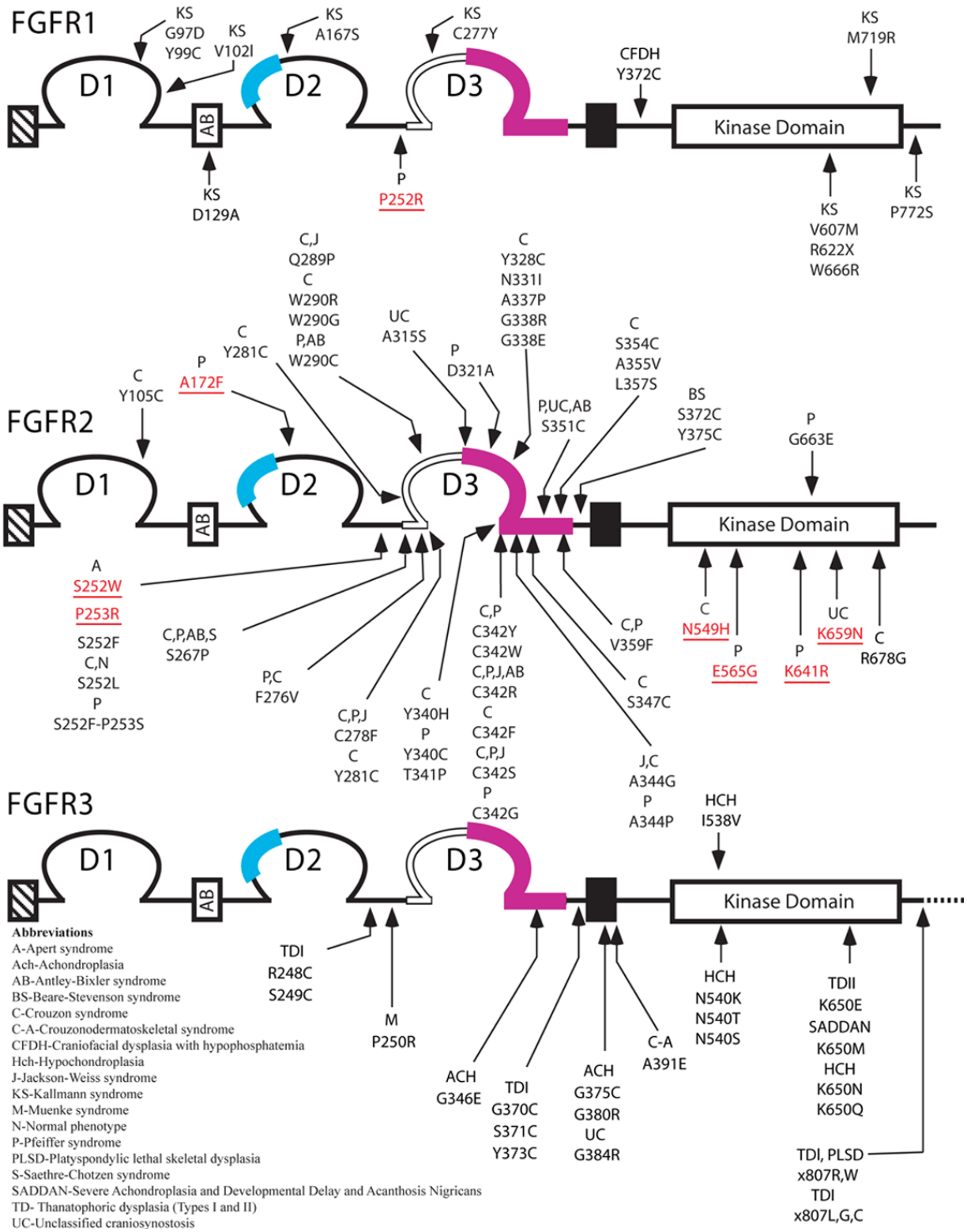

Figure 4. Pathogenic missense mutations within FGFR1, 2, and 3. Mutations whose mechanisms of action have been elucidated are in red letters and underlined. Taken from http://www.med.nyu.edu/mohammadi/LabPage/fgfr_mut.html

TWIST1

TWIST1 mutations have been found to cause Saethre-Chotzen syndrome, an autosomal dominantly inherited disorder involving a coronal synostosis phenotype, ptosis, widely spaced eyes, and minor abnormalities of the hands and feet (Robin, et al. 1998). This protein functions within the cell nucleus as a transcription factor and contains two nuclear localization signal sequences. Mutations within this gene cause the protein to either translocate to the nucleus by itself or inhibit its ability to enter the nucleus at all. TWIST1 received its name due to a complete eversion of the head seen in homozygous mutations of *Drosophila* (Lattanzi, et al. 2012). Due to the prevalence of FGFR2 and FGFR3 mutations seen within individuals with Saethre-Chotzen syndrome, it is speculated that TWIST1 is required for FGF signaling. Previous studies have shown that as TWIST1 levels decrease, FGFR distribution is altered, causing a reason to believe they are located within the same pathway (Rice, et al. 2003). TWIST1 is also thought to perform a regulatory role for BMP, and TGF-β signaling (Qin, et al. 2012). Mutations have been found in unaffected parents, showing a high variability of expression and reduced penetrance of TWIST1 mutations (Lattanzi, et al. 2012).

MSX2

The first mutation identified for a craniosynostosis phenotype was a heterozygous MSX2 missense mutation. MSX2 encodes a homeobox-containing transcription factor and a missense mutation P148H acts to stabilize DNA binding (Neilson, et al. 1995). This mutation was originally identified in a large three generation family containing 13 affected individuals. These individuals had a rare syndrome, later named Boston-type craniosynostosis for the location of the originally described family. Boston-type craniosynostosis is a highly penetrant autosomal dominant disorder that presents with forehead retrusion, frontal bossing, turribrachycephaly, and

the Kleeblattschaedel deforming (trilobular, or cloverleav) skull anomaly. None of the individuals in the family had any hand or foot abnormalities. It has not been documented which sutures were fused within each individual, but severity increased with each generation (O'Niell, et al. 2013).

Genetics of Nonsyndromic Craniosynostosis

Genetics of Nonsyndromic Craniosynostosis

FGFR – Coronal Synostosis

As stated previously, FGFR3 P250R mutations have been associated with isolated coronal synostosis, as well as Muenke syndrome. In one study, 4 out of 37 individuals with isolated coronal synostosis were found to have an FGFR3 P250R mutation. Although it is rare to see a familial trend with isolated synostosis, 3 out of these 4 individuals had a father with the same change, leading to the possibility of reduced penetrance of this mutation (Gripp, et al. 1998). Another study found an FGFR3 P250R mutation in 29 out of 76 individuals with isolated coronal synostosis (Thomas, et al. 2005). FGFR2-related isolated coronal synostosis has also been shown to link FGFR2 mutations to a specific NSC presentation.

FREM1 – Metopic Synostosis

One gene known to be associated with nonsyndromic metopic craniosynostosis is FREM1. FREM1 encodes an extracellular matrix protein that plays a role in epidermal differentiation, craniofacial development, and renal development. FREM1 stands for FRAS1 (Fraser syndrome 1 homolog) related extracellular matrix 1. FRAS1 encodes a protein that functions to regulate epidermal-basement membrane adhesion and organogenesis during development (Pavlakis, et al. 2011). One study of 109 patients with metopic craniosynostosis identified 5 *de novo* CNVs and 3 missense mutations in the FREM1 coding region (Vissers, et al.

2011). Further analysis of FREM1 in mouse models showed localization of the protein around the posterior frontal suture, the equivalent to the metopic suture. This finding was further confirmed by premature fusion of this suture in two different mouse lines carrying distinct FREM1 loss-of-function mutations. It is speculated that FREM1 can also bind FGFs via chondroitin sulfate proteoglycan repeats of the NG2 proteoglycan in the FREM1 protein (Vissers, et al. 2011).

Zebrafish as a Model Organism

One model organism that has been used for craniosynostosis studies is the zebrafish (*Danio rerio*), a small freshwater cyprinid fish. The zebrafish is a powerful model organism often used to study vertebrate embryogenesis, morphogenesis, and gene function (Quarto, et al. 2005). In contrast to mouse embryos, zebrafish develop *ex utero*, or outside the mother's body, allowing for visual analysis of early developmental processes. In addition to the external development, the craniofacial elements lie below a thin layer of tissue, allowing them to be easily observed in both fixed and live animals. Zebrafish also have short generation times and high fecundity, allowing for rapid genetic analysis (Dooley, et al. 2000). Moreover, a high degree of genetic and developmental conservation exists between zebrafish and humans (Grova, et al. 2012).

Zebrafish skulls have frontal, parietal, and occipital cranial bone elements with associated sutures, similar to those found in mammals (Figure 5). Also similar to mammalian development, the skull bones form via intramembranous ossification where the frontal bones are neural crest derived and the parietal bones are mesoderm derived. Interfrontal, sagittal, coronal, and lambdoid sutures are all found in the zebrafish skull in an arrangement similar to vertebrate organisms. In contrast to humans, the most anterior portion of the zebrafish skull remains patent

(Grova, et al. 2012). Osteogenesis is first detected around 27 days post fertilization (dpf), beginning at the frontal bone, and is completed by day 51. However, pre-patterning of the cranial sutures in the mesenchyme can be seen at 21 dpf, as shown in Figure 6. In zebrafish, cranial suture patterning is an active autonomous process, independent of osteogenesis, although, the cranial sutures can easily be detected prior to onset of osteogenesis (Quarto, et al. 2005).

What is known about craniosynostosis studies in zebrafish involves the study of a heterozygous mutation of cytochrome P450, family 26, subfamily B, polypeptide 1 (CYP26B1), an enzyme responsible for retinoic acid degradation. Retinoic acid has been well documented to have teratogenic effects in the limb and craniofacial skeleton. This study showed that zebrafish with this mutation developed coronal synostosis. Retinoic acid functions as a morphogen, establishing concentration gradients over all developmental fields in the developing embryo. A predicted model for retinoic acid function is that high levels promote osteoblast to osteocyte transitioning to produce terminally differentiated osteoclasts. Without the negative regulation of CYP26B1, accelerated maturation of the osteoblast cells to osteoclast cells could cause mineralization of the structure, causing craniosynostosis when it occurs in the skull bones (Laue, et al. 2011).

The zebrafish is an organism that will provide an opportunity to gain more insight into the molecular mechanisms governing skull development and cranial suture patterning.

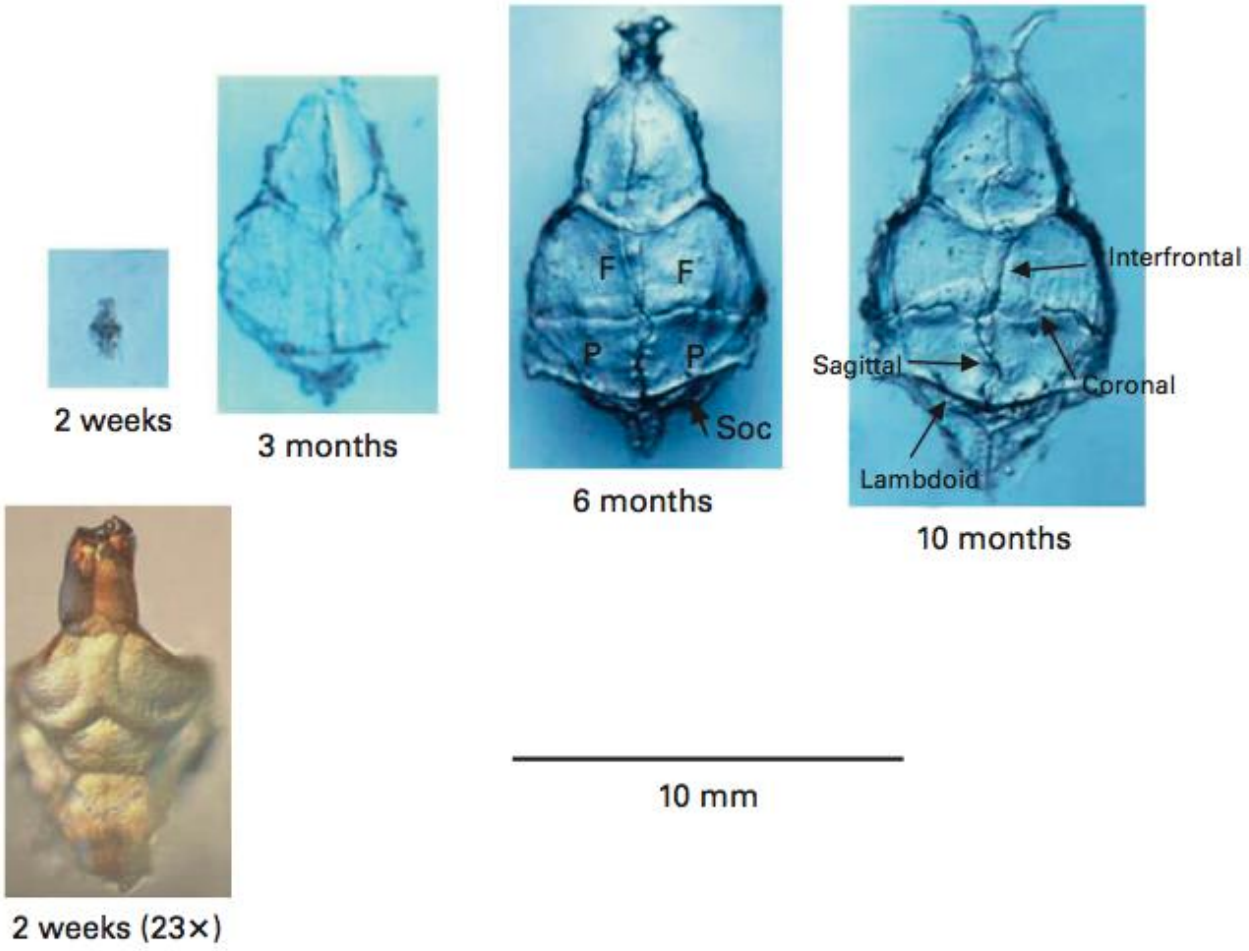

Figure 5. Morphology of zebrafish skull vault. Skulls were dissected from larvae, juvenile and adult zebrafish and analyzed under a stereomicroscope. Note the cranial sutures (arrows) and the frontal bone (F), parietal bone (P), and supraoccipital bone (SOC) of the skull vault. Taken from Quarto, et al. 2005.

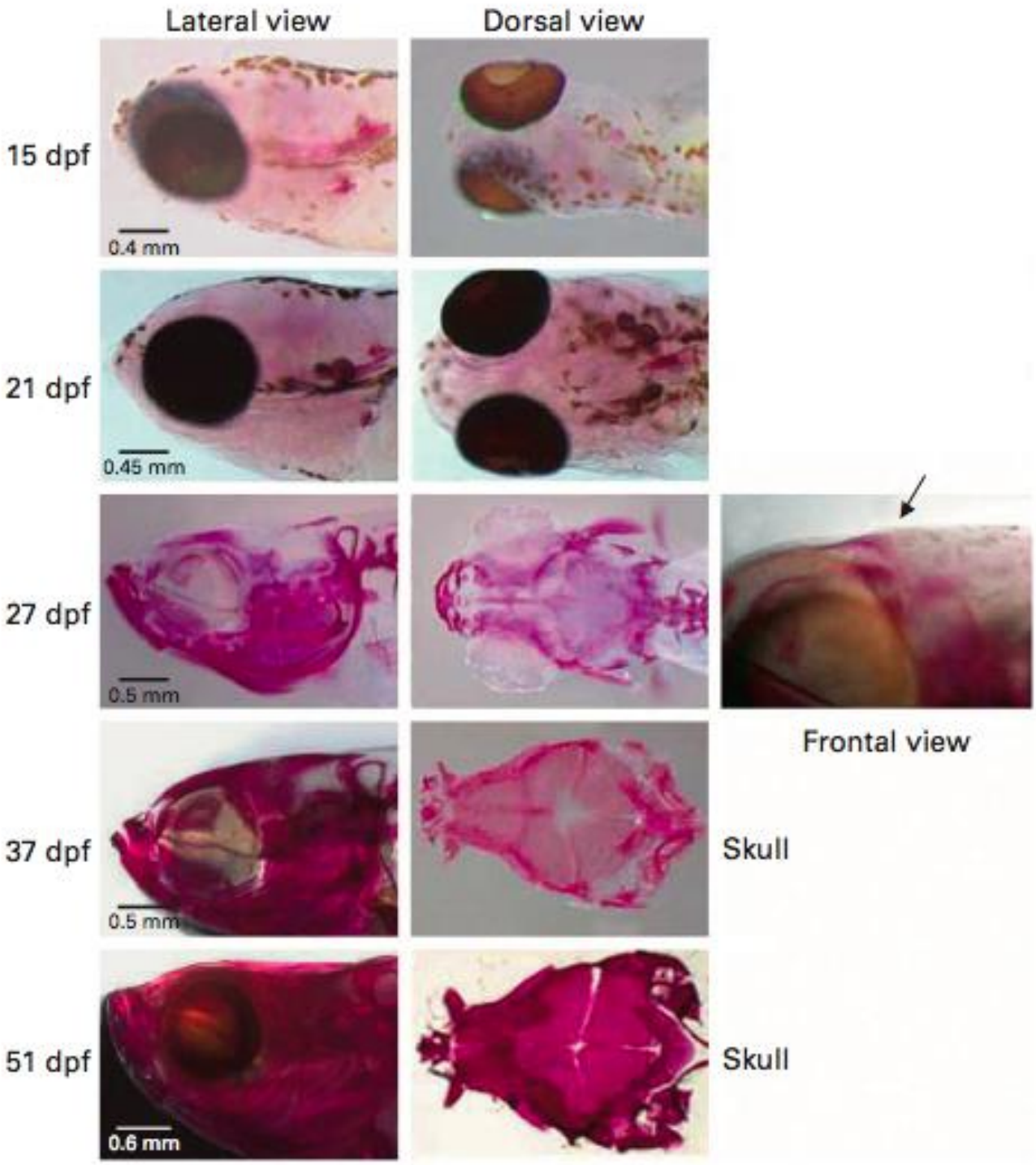

Figure 6. Calvarial bone osteogenesis. Larvae and juvenile zebrafish were fixed in 4% paraformaldehyde and stained with Alizarin Red to detect bony tissue. Note the presence of ossification (arrow) starting from the most anterior part of the skull (frontal bone) in 27-dpf specimens. At 51 dpf, complete bone maturation of the skull vault is observed. Taken from Quarto, et al. 2005.

Whole Exome Sequencing

Whole exome sequencing (WES) is a next-generation sequencing technique that has the potential to uncover the causes of a large number of rare, mostly monogenic disorders, as well as predisposing variants in common diseases and cancers. Human exomes constitute approximately 1.5% of the genome, but contain approximately 85% of disease causing mutations in monogenic disorders. Compared to whole genome sequencing (WGS), the cost is much lower, leading to a practical application in clinical genetic diagnostics (Rabbani, et al 2014). However, WES is primarily focused on the coding regions and splice-site variants in annotated genes, which creates the possibility for a missed mutation in a region of noncoding RNA, epigenetic regulation, control sequences, intronic regions, mitrochondrial DNA, or uniparental disomy.

Ethical concerns over WES include how much information the patient should be given regarding the results. For example, how many relatives of the patient should be informed? Or if a mutation identified could lead to increased susceptibility for a late-onset disease, should they be informed? As WES becomes cheaper and more clinically available, insurance companies could take advantage of the information, leading to higher premiums for patients who have the potential to develop a certain disease later in life (Rabbani, et al. 2014).

Although there are ethical and legal concerns over WES, the ability to identify a majority of disease causing mutations is a significant advancement in the medical world and provides the possibility of personalized medicine in the coming years.

Aims

The goal of this study is to provide insight into possible causes of craniosynostosis through the evaluation and analysis of several affected individuals and their families. After analysis of each individual's genome, several candidate genes will be located and investigated to

determine the likelihood of their involvement in skull and suture development. Final steps will involve model organism testing to determine whether mutation of each candidate gene causes a phenotype similar to that of craniosynostosis in humans.

Chapter 2: Materials and Methods

Patients

Patients affected with craniosynostosis were ascertained from the Virginia Commonwealth University Center for Craniofacial Care under the direction of Dr. Jennifer Rhodes. Blood samples were obtained from each patient, as well as available family members. Of the 100 samples that have been collected, 18 were used for this study. Patient samples were labeled with CS and a number correlating to the order in which they joined the study.

This study analyzed a three-generation family that included an affected son (CS-58), affected mother (CS-59), unaffected father (CS-60), and affected maternal grandmother (CS-61) (Figure 7a). CS-58 presented with left coronal, left lambdoid, and squamous synostosis. He also had scalloping of the occipital bone and an unusually large anterior fontanelle. This patient had normal hearing, but low set ears. He showed no evidence of midface hypoplasia, but his palate was slightly arched and his left eye displayed ptosis with mild proptosis. This patient was diagnosed clinically as having atypical Crouzon based upon these findings and the absence of limb abnormalities. The affected sutures of the mother and maternal grandmother are unable to be ascertained for our study due to the natural fusion of the skull bones over time, obscuring the premature fusion of specific sutures. Genetic testing of CS-58 screened for FGFR3 mutations, with no mutations found.

Two trios were also involved in this study. The first trio included a set of unaffected parents (CS-54 and CS-55) with their affected daughter (CS-39) (Figure 7b). CS-39 was born with complex synostosis involving the metopic, bicoronal, and lambdoid sutures. She also presented with proptosis, a tense and bulging fontanelle, midface hypoplasia, subsquamosal bulging, noisy breathing with gurgling, Chiari malformation, and turricephaly with a coned superior occiput and flattened lower occiput. In addition to her craniofacial abnormalities, she

struggled with delayed gastric emptying, seizures, and kyphosis of her lower thoracic/upper lumbar spine. She was diagnosed as having Pfeiffer Type 3. Genetic screening was performed on CS-39 in order to test for TWIST1 mutations, FGFR1 P252R mutation, FGFR3 P250R mutation, and sequencing of FGFR2 exons 3a, 3c, 8, and 10. All results revealed no mutations. The second trio family included an affected father (CS-65), unaffected mother (CS-66), and affected daughter (CS-64) (Figure 7c). CS-64 was born with sagittal synostosis, and it is believed that CS-65 was also affected with sagittal synostosis based upon his clinical appearance. No genetic screening of CS-64 or CS-65 was performed.

We also included CS-14 and CS-15, a pair of monozygotic twins discordant for craniosynostosis (Figure 7d). CS-14 was born affected with nonsyndromic sagittal synostosis. No genetic screening had been performed on the twins.

Also included in our study was a family of six individuals, including an unaffected mother (CS-7), unaffected father (CS-2), and four of their children (CS-3, CS-4, CS-5, CS-6) (Figure 7e). CS-3 and CS-4 were born affected with sagittal synostosis. CS-5 was born with midline cutaneous meningioma, but did not present with a craniosynostosis phenotype. CS-6 is unaffected. No genetic screening of this family was performed.

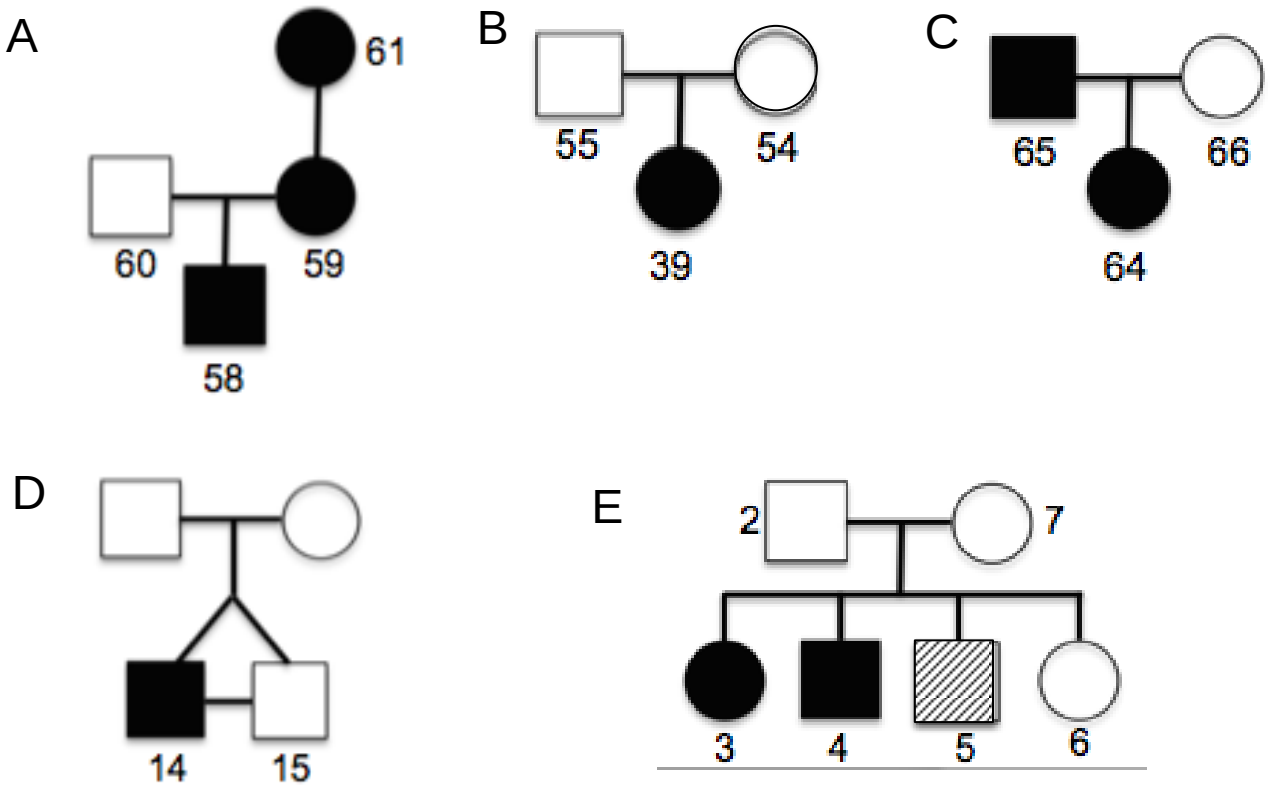

Figure 7. Pedigrees for (A) three generation family CS-58, CS-59, CS-60, and CS-61 segregating craniosynostosis in an autosomal dominant pattern; (B) trio family CS-39, CS-54, and CS-55; (C) trio family CS-64, CS-65, and CS-66 with autosomal dominant segregation; (D) monozygotic twins CS-14 and CS-15; (E) family of six with CS-2, CS-3, CS-4, CS-5, CS-6, and CS-Filled in circles are affected individuals. The hatch marked square is the individual with cutaneous midline meningioma. Arrows indicate the proband of each family

Whole Exome Sequencing

Whole exome sequencing for all individuals, excluding the six-member family, was performed by Beckman Coulter Genomics, Inc. A hard drive was provided including the variant call format (vcf) files, Standard Alignment and Mapping format (SAM file), and Binary Alignment and Mapping format (BAM file). The BAM file is a compressed version of the SAM file and both contain aligned and non-aligned reads. Beckman Coulter Genomics, Inc uses Agilent SureSelect V5 target capture covering approximately 50Mb.

Sequence mapping was performed on a genome reference sequence using the Burrows-Wheeler Alignment tool (BWA) version 0.6.1-r104 with default parameters. Library fragment sizes from the BWA mapping were estimated with Dindel version 1.01 using default parameters. Read map proportions are estimated using samtools version 1.18 "view" command with a BED file reflecting the extent of the baits present in the target enrichment kit used, the hsV5 kit. Table 3 statistics are obtained using bamtools version 2.2.3 "stats" command. Table 4 duplicate read pairs are estimated by PICARD version 1.86 "MarkDuplicates", samtools "Rmdup", and FastQC. "Pairs needed" is obtained by extrapolating the average coverage with duplicates resulting from the sequence pairs generated, for libraries not reaching the quoted coverage.

Whole exome sequencing for the six member family was performed by the Nucleic Acid Core. Dr. Todd Web performed the quality control and mapping, and Dr. Tim Bigdeli did the filtering. Filtering was performed to include recessive and spontaneously inherited alleles. Quality control filters were similar to the ones described for all other families.

Mendelian Error Analysis

Analysis to determine relationships between family members Mendelian errors was performed using the "plink" program. This program outputs several files detailing the nature of

any Mendelian error found within each family. In order to determine if the number of errors within a family significantly differed from the number of errors in an unrelated family, three simulations were run. Each simulation used a fake pedigree file using the proband of each family (CS-39, CS-58, or CS-64) with unrelated parents. An example of a fake pedigree file is shown in Table 2a and compared to the real pedigree shown in Table 2b, where a 0 indicates a missing value. The mean of the three trials was calculated and used to run a one tailed t-test against the number of real Mendelian errors found. Mendelian errors were performed with the raw data prior to any filtering.

For the CS-14 monozygotic twin pair, past twin studies were used to compare the amount of errors found after quality control filtering. Plink Mendelian error analysis was unable to be performed on this family because parental data is required and not available

Table 2a

Individual	Family	Father	Mother
CS-39	1	CS-65	CS-61
CS-65	1	0	0
CS-61	1	0	0
CS-64	2	CS-15	CS-54
CS-15	2	0	0
CS-54	2	0	0
CS-58	3	CS-55	CS-66
CS-55	3	0	0
CS-66	3	0	0

Table 2b

Individual	Family	Father	Mother
CS-39	1	CS-55	CS-54
CS-54	1	0	0
CS-55	1	0	0
CS-64	2	CS-65	CS-66
CS-65	2	0	0
CS-66	2	0	0
CS-58	3	CS-59	CS-60
CS-59	3	0	0
CS-60	3	0	0

Filtering of Variants

KGGseq was used for prioritization of causal variants within each individual's exomes. KGGseq uses a three-level filtration framework to organize the variants. The first level of filtration is at the genetic level. This level excludes variants outside of identity by descent (IBD) regions and variants conflicting with disease inheritance patterns. The CS-14 twin pair was filtered to search for any variants that differed between the twins using the *de novo* filter. The CS-39 trio was filtered to include only recessively inherited homozygous alternate alleles and *de novo* mutations. Both the CS-64 and the CS-58 families were filtered to include dominantly inherited heterozygous alleles. Also within this filtration level are quality control boundaries in order to ensure each variant that is kept adheres to the quality standard set by the user.

The second level of filtration is the variant-gene level, which further analyzes each variant kept from the genetic level. The primary purpose of this level is to filter out mutations that are unlikely to cause diseases. This involves the comparison of the variants with information pulled from the 1000 Genomes project, dbSNP database, and/or NHLBI GO Exome Sequencing Project. Genome builds available for comparison are hg18 and hg19. This project used the hg19 build and compared variants using dbSNP138, NHLBI GO Exome Sequencing datasets of African Americans and European Americans, and all samples within the 1000 Genomes project from the April 2012 release. Minor allele frequencies can be set manually prior to filtration. The minor allele frequency (MAF) was set at 0.01 for each family but the CS-64 trio. Due to the large amount of variants found after genetic level filtration, the MAF for this trio was set at 0.005. Variants are then mapped using Refseq to determine where the variant lies within the genome, and can be excluded based on the user's specifications.

The final level of filtration is the knowledge level. KGGseq incorporates physical protein-protein interaction from the STRING database to determine which variants will be the

most deleterious based upon their function. KGGseq allows the user to input a set of candidate genes to determine if the gene containing the variant interacts within the pathway of the candidate. Another optional feature of the knowledge level filtration is the capability to input certain words that can be searched for in the NCBI PubMed database.

An example of a KGGseq script and candidate gene list is shown in Figure 8. Exact scripts used for each family are shown in Appendix I. After all variants have been filtered, an annotated excel document is output that can be filtered further based upon the user's specifications. For this project, the resulting excel document for each family was evaluated and prioritized. Variants were kept that fell into the classification of missense, frameshift, splicing errors, stoploss, and stopgain. This excluded synonymous, intronic, intergenic, ncRNA, and nonframeshift mutations.

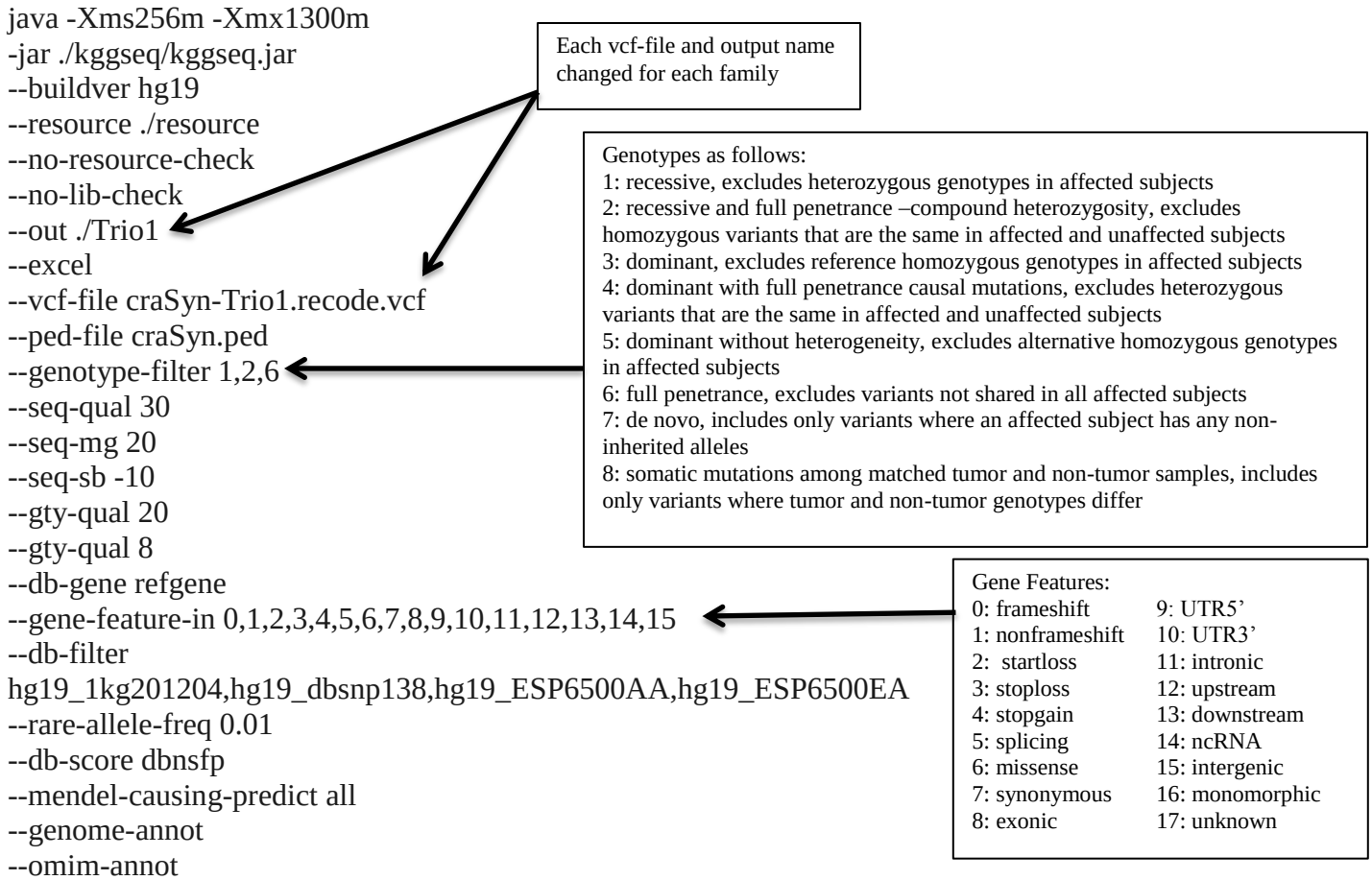

Figure 8. KGGSeq script used to filter each individuals vcf file. Filters changing between families are shown in the boxes.

Quality Control of Variant Calls

Once variants were identified via KGGseq filtering, further analysis was performed through the Integrated Genome Viewer (IGV) available from www.broadinstitute.org/igv/home. The IGV allows real time exploration and analysis of large-scale genomic datasets on standard desktop computers. Each individual's genome (BAM file) was loaded into the software and compared to the USCS hg19 build. Candidate variants were localized by using the chromosome number and position from the KGGseq output. Variants were then compared between family member and determined whether there was enough evidence to further analyze the gene. IGV quality control is a check based to determine that each variant identified has an adequate amount of reads to support the mutation found through KGGseq. An example of the view from the IGV is shown in Figure 9.

Figure 9. View of a BHMT variant in the IGV. View in the top left shows the genome build, chromosome number, and specific location on the chromosome. Along the left side are the names of the individuals being analyzed. Along the bottom of the figure are the sequence and the corresponding amino acid according to the RefSeq database. Hovering above the specific base will allow more information to be seen, as shown in the tan box.

PCR Primer Design

Primers for PCR and Sanger Sequencing of each gene were designed using the aid of IDT Primer Quest (http://www.idtdna.com/Primerquest/Home/Index) and ordered via IDT using Custom DNA Oligo Service. The Thermo Scientific Phire Hot Start II DNA Polymerase was used for all PCR reactions. Primers, annealing temperatures, and product sizes for each gene are shown in Table 1. PCR conditions were as follows: 94º C 1.5 min, (94º C 30 sec, annealing temp 30 sec, 72º C 30 sec) x29, 72º C 7 min. PCR products were run on 6% acrylamide (19:1) and 10% glycerol gels in 0.5X TBE and visualized using ethidium bromide as a staining agent. As shown in Table 3, a reverse primer was unable to be obtained for FGFR3. Four different primer sequences were attempted. For the FGFR3 forward sequencing, a primer was used that amplified inside the PCR product. This primer sequence was: GCAGCCGAGGAGGAGCTGGTGG

Table 3

Gene	Forward Primer 5 -> 3'	Reverse Primer 5 -> 3'	Temp	Size
BHMT	TCCTGATGAAGAGAGGAGAGCTG	GACAGAAACCAGGGACAAGAC	64	400
C11orf34	GCACTGGAGAAGGGTTGATTG	TGTTTTGGTCTGAAGCCGTG	60	472
CCT4	AGTTAGCAGGTTATTCAAGCCAC	ACAGTTACCTAGCCACTCTTG	67	421
FGFR2	GGGGGTATCCTCTGGTTGCT	ATGGCTACAGAGAAGAGAGAGC	60	511
PTPN7	AGCCTTGGGTTCTTTGTGGG	GCCCTCTTATATCCCCGGAGT	60	475
RNF157	AGCAGGATCTACAGTGTGTGA	GGAACAGCCCAGAGGGTTAC	60	537
TRDN	ACTTGTGACTTACCTTTCTTCCC	GATGCTACCTCCAAACCCCTT	60	554
TSPG1	TCAAAGCCTGTCGTGTGGAT	ATCCAGTTCACGTAGGCAGG	64	551
ZNF516	CAGGTCAGGGGGTCTTCGC	CCACCACGTCTTGTTCTGACA	65	502
FGFR3	ACGGACGGGAATCCTGTGA	CTACATGGTGAAGCAGAGACGA	60	480
BAMBI	CTAGGAGGAGTTAGCATGGAG	CTTCAAGCTGTTCAGTAAGTG	60	508
CRELD1	GGTCGCTGTAAGAAGTGTAG	CCTGGAAGGTATAAGGCTGC	60	588
ITGAV	GTAACCCTGAACTTGCCTTAT	GTGCCTATGAGCTCCCTATTC	65	685
SLC20A1	CTCCTTGTCCAAACAGTCTC	GCTCTGTCAAACGGCTCTTC	60	624
SLC30A9	GGTTATAACACAACCTGCTTC	GATATGTAAGAGCCACACAGG	60	524
AR	GCCAAGCTCAAGGATGGAAG	CCTCGCTCAGGATGTCTTTA	60	710
HRNR	CATCACTCTCTTGCTACATGG	CTCTCACCAAGTAAGGACAATC	60	461
FREM1 Ex15	CTGTCTTCAGGGGTCATGGAA	CTGACCCGTTGAGTGTGTTA	60	405
FREM1 Ex26	GCAAGATCTGCCCTTGATT	CCTTGGTTTGTCCCATCTG	60	502

Sanger Sequencing

PCR volumes for Sanger Sequencing were cleaned using ZymoResearch DNA Clean and Concentrator. All Sanger sequencing reactions were performed by the MCV-VCU Nucleic Acids Research Facility using the BigDye Terminator v3.1 mix and the primers shown in Table 1. Results were viewed using Chromas Lite 2.1.1.

In Silico Functional Prediction of Candidate Genes

Analysis of the candidate variants within the CS-64 family was performed using the aid of Project HOPE, run by Netherlands Bioinformatics Centre (www.cmbi.ru.nl/hope). Project HOPE uses Basic Local Alignment Search Tool (BLAST) to search the Uniprot database and the Protein Data Bank (PBD). PBD is used to find the 3D structure of the protein of interest, or a possible template for homology modeling. Multiple other programs are integrated into Project HOPE to build the structure of the protein, determine the domains and motifs within each structure, and analyze any known variants within the sequence. This information is then combined to analyze the effect of certain mutations on the protein structure and stability.

CRISPR/Cas9 Clone Generation

CRISPR targets and sequencing primers for the targets were obtained using the aid of https://chopchop.rc.fas.harvard.edu/. CRISPR guide RNAs (gRNA) were designed according to the protocol “short oligo method to generate gRNA” taken from Talbot and Amacher (2013). Three gRNAs were designed for each candidate knockdown gene (SLC30A9 Guides 1, 2, and 3, and ITGAV Guides 1, 2, and 3) due to the known approximate 50% success rate of CRISPR guides. Each guide RNA included a clamp, T7 promoter, target sequence, and an overlap with the guide constant oligo. All gRNA, gRNA Primer 1, gRNA Primer 2, and guide constant oligo were obtained through IDT. Primer sequences are show in Table 4 a and b.

PCR amplification of template oligos was performed using the protocol from Talbot and Amacher (2013). The PCR was run with 1x Thermopol buffer, 0.25 µM each gRNA Primers 1 and 2, 0.02 µM short-guide oligo, 0.02µM guide constant oligo, 3% DMSO, 0.2 mM dNTPs, and 1.5 units Phire Hotstart II DNA Polymerase. Two 50µl reactions were run with the following cycling parameters: 95º C 1 min (95º C 15 sec, 60º C 30 sec, 72º C 20 sec) x40, 72º C 5 min. PCR amplified products were confirmed by visualization of a 120 bp band run on a 6% acrylamide (19:1) and 10% glycerol gels in 0.5X TBE using ethidium bromide as a staining agent

Transcription of the gRNA was carried out via Ambion MEGAScript Sp6/T7 kit, following the manufacturer's instructions, then cleaned using the MirVana miRNA Isolation Kit. The final concentration for each gRNA was diluted to 200 ng/µl for injections.

Table 4a

Name	**Sequence**
SLC30A9 Guide1	GCGTAATACGACTCACTATAGGTGCAGGTAGACCCGGCAGGTTTTAGAGCTAGAAATAGC
SLC30A9 Guide2	GCGTAATACGACTCACTATAGGCAGGTATCAGCCAACGAGGTTTTAGAGCTAGAAATAGC
SLC30A9 Guide3	GCGTAATACGACTCACTATAGGAGGACTGACCTGACAGCGGTTTTAGAGCTAGAAATAGC
ITGAV Guide1	GCGTAATACGACTCACTATAGGCCCCAGAGGAACGCACAGGTTTTAGAGCTAGAAATAGC
ITGAV Guide2	GCGTAATACGACTCACTATAGGGGCTCAGATGGCAAACTGGTTTTAGAGCTAGAAATAGC
ITGAV Guide3	GCGTAATACGACTCACTATAGGTTCATCGCAGAGACCTGGGTTTTAGAGCTAGAAATAGC

Table 4b

Guide Constant Oligo	AAAGCACCGACTCGGTGCCACTTTTTCAAGTTGATAACG GACTAGCCTTATTTTAACTTGCTATTTCTAGCTCTAAAAC
gRNA Primer 1	GCGTAATACGACTCACTATAG
gRNA Primer 2	AAAGCACCGACTCGGTGCCAC

Table 4 Key:Red color denotes the clamp, blue is the T7 promoter, black is the target sequence, and green is the overlap with the guide constant, as well as the sequence on the guide constant that overlaps.

Generation of BAMBI Overexpression Clone

Zebrafish have two orthologues for the BMP and activin membrane-bound inhibitor (BAMBI) gene (orthologues a and b). Although little is known about the Bambi genes in zebrafish, it is thought that the two orthologues perform the same function with slightly different amino acid sequences. Bambia was chosen for overexpression studies due to its commercial availability. The cDNA clone of the Bambia gene in pBluescript SK- was ordered through http://dharmacon.gelifesciences.com (Appendix II). After arrival of the BAMBIa vector glycerol stock, the bacteria was streaked on an Ampicillin (Amp) Luria broth (LB) plate and grown overnight at 37º C. A 4 ml LB with 0.2 mg/ml Ampicillin overnight was prepared and shaken overnight at 225 rpm and 37º C. After ensuring bacterial growth had occurred, the Thermo Scientific GeneJET Plasmid Miniprep Kit was used to isolate the DNA.

A heat shock promoter vector (pCSHSP) was obtained from Dr. James Lister (Appendix II). Both vectors (pCSHSP and BAMBIa) were digested in a 50 µl reaction using 50 units of BamH1 20 u/µl (Appendix II), 1x New England Biolabs (NEB) Buffer 3.1, and 5 µg of DNA. The digest was incubated at 37º C for 1 hour. Confirmation of the digest was visualized on a 1% agarose gel run in 1X TAE using ethidium bromide as a staining agent. After complete digestion was confirmed, the rest of the samples were run on a 1% agarose prep gel. The band containing the BAMBIa insert and the cut pCSHSP vector were excised and purified using the BioRad Freeze N' Squeeze DNA Gel Extraction Spin Column. Dephosphorylation of pCSHSP was performed in a 32 µl reaction using 1 unit/pmol Roche Shrimp Alkaline Phosphatase (SAP), 1x SAP buffer, and 1.36 µg of DNA. The reaction was incubated at 37º C for 10 min, then 65º C for 15 min. The pCSHSP dephosphorylated vector and the BAMBIa insert were then ligated in a 10 µl reaction using NEB 40 units of T4 ligase, 1x NEB T4 ligase buffer, and a 3:1 ratio of insert:vector with 50 ng of vector. The ligation reaction was incubated overnight at 14-15º C. A

control without the BAMBIa insert was ligated to determine the effectiveness of the dephosphorylation step.

Transformation into DH5α cells was performed as follows. Fifty microliters of supercompetant cells were gently thawed on ice and aliquoted into 50 µl tubes. Two microliters of the ligation reaction was added and mixed gently by tapping the tube. Cells were incubated on ice for 30 min, heat shocked for 40 seconds at 42º C, then placed on ice for 2 min. Nine hundred fifty microliters of room temperature LB was added to the 50 µl transformation mix and shaken at 225 rpm and 37º C for 1 hour. A volume of 100 µl of transformation mix was spread on an LB Amp plate to grow overnight at 37º C. Ten colonies were individually isolated and 2 ml overnights in LB and 0.2 mg/ml Amp were grown overnight at 225 rpm and 37º C. The plasmid DNA from each overnight was isolated using the Thermo Scientific GeneJET Plasmid Miniprep Kit, as above. A small amount (5 µl) of each plasmid was digested with BamH1 and run on a 1% agarose gel to identify if the correct insert had been cloned. Three plasmids with the correct insert size were sent for sequencing using the SP6 primer to ensure the cloned DNA was in the proper orientation with no mutations.

Zebrafish Culture and Maintenance

Adult fish were maintained at approximately 28°C on a 14 hour/10 light/dark cycle. Wild type strains (AB/ WIK or ZIRC AB) were used for all experiments unless otherwise indicated. Embryos were incubated at 28°C and staged according to Kimmel et al. (1995).

Zebrafish Injection

Injection trays were made using 0.45 g agarose and mixed with 30 mls of system water. The mixture was microwaved for 1 min to melt the agarose and then cooled at room temperature for 10 min. Thirty microliters of methylene blue solution was added and then the mixture was

poured into a 10 cm petri dish. The injection tray mold was set on top of the fluid while solidifying. Injection trays are stored at 4º C until needed. Injection needles are created using the Sutter P-97 Flaming/Brown micropipette puller on program 6.

Zebrafish males and females were separated into spawning tanks the evening before injections were to be performed. The morning of injections, fish are placed in a new spawning cage with fresh water and the divider is pulled out, allowing the males and females to mate. Injections were performed within 10 min of fertilization of the eggs. Approximately 40 embryos were injected for each target, aside from the control where 80 embryos were injected. Control fish were injected with only a the CRISPR protein. A mixture of 200 ng/µl of each CRISPR was mixed with 200 ng/µl of the Cas9 protein, to have a final concentration of 100 ng/µl of each vector. Each embryo was injected with approximately 1 nl of the mixture.

Staining

Staining of the zebrafish was performed via the Clearing and Staining for Larval Fish Cartilage and Bone protocol from ZFIN (Potthoff, et al. 1984). Fish were stained at 5 weeks and 8 weeks old. Once fish had reached the desired age, they were euthanized with Ethyl 3-aminobenzoate, methanesulfonic acid salt 98% (MESAB), then fixed in 4% paraformaldehyde in PBS for 48 hours at 4º C. After fixation, fish were rinsed in two separate 5 minute PBS washes, dehydrated in 50% EtOH for 24 hours, then in 100% EtOH for 24 hours. Cartilage staining then proceeded with a 24 hour room temperature incubation with mild agitation in a 100 ml solution of 70% EtOH, 30% acetic acid, and 0.2 mg/ml Alcian blue. Fish were then neutralized in a saturated sodium borate solution for 9-12 hours and bleached for 20 min in a 100 ml solution of 15% 3% hydrogen peroxide and 85% 1% potassium hydroxide. A trypsin digest followed involving a mild agitation wash in 35 ml saturated sodium borate, 65 ml ddH_2O, and 1 g trypsin

until the specimens were 60% clear. Bone staining then proceeded with a 24 hour room temperature incubation with mild agitation in 1% potassium hydroxide and 1 μg/ml Alizarin red. Another trypsin digest then occurs for 40-48 hours. Preservation, the final step, proceeds at room temperature with a solution containing 30% glycerol and 70% 1% potassium hydroxide for 2-3 days with mild agitation, then a solution of 60% glycerol and 40 % 1% potassium hydroxide for 2-3 days with mild agitation, and finally a 100% glycerol solution.

Genotyping

In order to identify mutation carries, DNA was prepared from fin clip biopsies and genotyped using PCR and Sanger Sequencing. PCR primers for the ITGAV Guide 1 and SLC30A9 Guide 3 are shown in Table 5. The other two ITGAV guide PCR primers ordered were not working properly and need to be redesigned. Once fish had reached the proper time points, listed above, and euthanized for staining, a triangular portion of the caudal (tail) fin measuring approximately 5mm on each side was clipped off using a clean razor blade. Using sterile forceps, this fin biopsy was place in 50 μl ZIRC lysis buffer (1.5 mM $MgCl_2$, 10 mM Tris-HCl pH = 8.3, 50 mM KCl, 0.3% Tween-20, 0.3% NP-40 (20%) in water). DNA was prepared by heating the samples in heat blocks through the following steps: 10 minutes at 95°C, followed by addition of 5 μl Proteinase K (10 mg/ml), followed by incubation at 55° C for 1 hour, and a final incubation at 95° C for 10 minutes to inactivate the Proteinase K. The tubes were then spun in a microcentrifuge and stored at -20° C

Table 5. PCR Primers for Sanger Sequencing of CRISPR/Cas9 Mutants

	Forward Primer	Reverse Primer
ITGAV Guide 1	GATGACAGAAAGCATTCCAATG	GCAGATGTTTTTATTCAGGT
SLC30A9 Guide 3	CTGCGTTTCTCATCTACACC	GCTTGTTGGCTGATTAAGC

Chapter 3: Results

Whole Exome Sequencing Analysis

Sequencing of all exomes from Beckman Coulter Genomics, Inc was completed with an average forward quality Phred score of 36.2 and an average reverse quality Phred score of 35.8. Exome and targeted region coverage details are shown in Table 6. Forward and reverse strand statistics refer to the exome. Target capture bait design is strand biased and target capture is strand specific. Reverse reads are, in general, of lower quality than the forward reads and as a result, there will be some strand bias. Most variant callers will filter out detected variants if observed on only one strand. The 'proper' pairs reported are read pairs mapped at expected distance and orientation, with regards to library size. Lastly, the on-target percentage reflects the proportion of reads overlapping the baits. Since, for instance, for exome design, over two hundred thousand regions are targeted, quite often, one of the two reads in a pair will be off target. Table 7 shows average coverage per sample, as well as proportions of the bait regions, having at least 5X and at least 10X coverage.

Table 6. WES Statistics

	Reads Generated	GC	Reads Mapped	Prop. Mapped	On Target	F Strand	R Strand	Strand Bias	Pairs Mapped	Proper Pairs	Single-tons
CS-14	84,371,026	45%	83,140,241	98.5%	64%	50.5%	49.5%	1%	98.1%	97.5%	0.5%
CS-15	73,436,098	46%	72,540,492	98.8%	66.6%	50.4%	49.6%	0.8%	98.4%	98%	0.4%
CS-39	98,934,296	45%	97,629,084	98.7%	66.7%	50.4%	49.6%	0.9%	98.3%	97.8%	0.4%
CS-54	89,719,978	46%	88,596,749	98.7%	70.3%	50.4%	49.6%	0.8%	98.3%	97.9%	0.4%
CS-55	90,868,512	47%	89,680,185	98.7%	68.1%	50.4%	49.6%	0.9%	98.3%	97.8%	0.4%
CS-58	89,545,620	46%	88,429,99	98.8%	66.1%	50.4%	49.6%	0.8%	98.3%	97.9%	0.4%
CS-59	89,952,862	47%	88,767,038	98.7%	69.6%	50.4%	49.6%	0.8%	98.2%	97.5%	0.5%
CS-60	87,584,168	47%	86,390,970	98.6%	67.3%	50.5%	49.5%	0.9%	98.2%	97.7%	0.4%
CS-61	83,960,342	46%	82,865419	98.7%	67.3%	50.4%	49.6%	0.9%	98.3%	97.7%	0.4%
CS-64	83,774,682	47%	82,629,412	98.6%	67.1%	50.4%	49.6%	0.9%	98.2%	97.6%	0.5%
CS-65	97,185,868	47%	95.713,982	98.5%	69.8%	50.5%	49.5%	1%	98%	97.5%	0.5%
CS-66	88.768,752	45%	87,434,774	98.5%	62.7%	50.5%	49.5%	1%	98%	97.3%	0.5%

Table 7. WES Average Coverage

	Library	Read Pairs	Avg.Cov.	>5X	>10X	PicardDupl.	SamtoolsDupl.	FastQCDupl.	MedianCov.	Pairs Needed
CS-14	IL7221	28,792,928	92.1X	97.6%	96.4%	9.6%	9.5%	25.5%	77.5X	2,469,752
CS-15	IL7222	30.141,652	83.6X	98.1%	96.8%	9.2%	9.1%	27.7%	71.6X	5,912,956
CS-39	IL7229	34.159,444	112.8X	97.7%	96.7%	15.4%	15.2%	33.5%	97.2X	0
CS-54	IL7230	30,822,168	108X	98.4%	97.5%	24%	23.8%	41.5%	93.4X	1,086,340
CS-55	IL7223	29,398,810	106.3X	98.8%	98%	12.8%	12.7%	28.8%	93.7X	0
CS-58	IL7224	29.510,856	101.2X	98.7%	97.8%	15.1%	15%	30.4%	87.6X	0
CS-59	IL7231	34,523,270	107.4X	98.9%	98.2%	13.5%	13.4%	33.6%	95X	0
CS-60	IL7225	23,623,880	101.1X	98.8%	98%	14%	13.9%	26.4%	89.1X	0
CS-61	IL7226	34,064,086	96.6X	98.3%	97.4%	14.2%	14.1%	33.8%	84.6X	1,198,943
CS-64	IL7227	31,934,591	96.1X	98.1%	97.2%	19.6%	19.4%	38.5%	85.9X	3,180,692
CS-65	IL7232	25,621,162	116.2X	99%	98.3%	14.6%	14.4%	27.8%	101.5X	0
CS-66	IL7228	30.707,133	95.2%	97%	95.8%	11.8%	11.7%	27.3%	83X	1,548,259

Mendelian Error Analysis

Results from the Mendelian error analysis are shown in Table 8. Errors from the analysis with the real pedigree file are shown in column two and the mean of the three simulation trials is shown in column three. Column four shows the p-value corresponding to the one tailed t-test. There are many more errors in the pedigrees when the parent genotypes have been simulated and there are significant differences between the real and simulated pedigrees.

For the CS-14 twin pair, 43 errors were found in non-intergenic and non-intronic areas of the exome sequencing. This makes up less than 0.001% of the exome sequencing performed.

Table 8. Mendel Errors

	Mendel Errors Real pedigree	Mendel Errors Mean of 3 Simulations	p-value One tailed t-test
CS-39 Trio	344435	509325	0.000144
CS-64 Trio	302148	431749	0.005361
CS-58 3 Generation	393672	637592	0.0092

KGGSeq and IGV Filtering

Analysis of the WES performed involved two main steps: KGGseq filtering and IGV quality control analysis. For the three generation CS-58 family, 113 variants were left after dominant KGG filtering. Mutations with no rsID were eliminated in order to narrow the search to novel mutations not yet identified, leaving 29 variants left. Further filtering kept only variants with a SIFT score of less than 0.5, as well as a Polyphen2_HDIV score greater than 0.957, leaving 15 total. These two tests were used to determine which variants are predicted to be the most deleterious. Twelve were kept after IGV analysis. The most significant variant identified was a missense mutation in the FGFR2 gene. According to RefSeq records, the mutation is located within exon 2 of NM_1144913, NM_1144917, and NM_1144914; and exon 3 of NM_00141 and NM_22970. Within each of these alternate sequences, an A314G mutation is seen. This corresponds to a Y105C amino change. The other eleven genes in which variants were found included MASP2, PTPN7, CCT4, ANKMY1, BHMT, TRDN, CIZ1, OR6T1, RNF157, and ZNF516. These mutations were included in further confirmatory tests in order to determine the efficiency of the WES.

For the CS-39 trio, *de novo* KGG filtering found 6 variants, and recessive filtering left 3 variants. After viewing each variant through IGV, 4 *de novo* and 2 recessive alleles remained. The most significant candidate variant was a *de novo* FGFR3 missense mutation. According to RefSeq records, the mutation is found in exon 9 of NM_00142 and NM_1163213. This mutation is C1172A, corresponding to A391E amino acidchange.

Filtering of the variants from the monozygotic twins, CS-14 and CS-15, left 7 variants. IGV analysis left two candidate genes, androgen receptor (AR) and hornerin (HRNR). The AR mutation is an A173T change found within exon 1 of RefSeq NM_000044, corresponding to a Q58L change. The HRNR mutation is found within exon 2 of RefSeq NM_001009931 causing

an A1T mutation, resulting in a M1L change. The twins were then filtered to determine if there were any mutations in both of their exomes that are known to cause craniosynostosis. No such variants were found.

Within the CS-64 trio, 143 variants were found after KGG filtering. In order to narrow down the candidate genes, variants with no rsID were kept in order to narrow the search to novel mutations not yet identified, dropping the number to 40. Further filtering included only variants with a SIFT score of less than 0.5 and a Polyphen2_HDIV score greater than 0.957. As with the CS-58 family, these two tests predict how deleterious the mutation is predicted to be. In the end, only 26 genes were left. Each of the 26 genes were analyzed to determine function and known embryonic tissue localization. Three variants, integrin alpha V (ITGAV) BAMBI, and solute carrier family 30, member 9 (SLC30A9), were left after analysis. Two additional variants were included in sequencing: SLC20A1 and CRELD1.

ITGAV has a missense mutation in exon 2 of NM_1144999, NM_1145000, and NM_002210. In NM_1144999, the mutation occurs at base 61. In the other two sequences, the mutation is at base 199. The mutation changes a cytosine to a thymine, leading to a leucine to phenylalanine change in the protein at amino acid 21 or 67, depending on the transcript. SLC30A9 has a missense mutation in exon 13 of RefSeq record NM_006345 causing C1079T, corresponding to a L360P change. The BAMBI gene has a mutation in exon 3 of RefSeq NM_012342 of A368G, leading to an M190V mutation.

Within the CS-2 six member family, 375 variants were found after KGG filtering. Further filtering included only variants with a SIFT score less than 0.5 and a Polyphen2_HDIV score greater than 0.975, narrowing the number to 84. The most interesting candidate was the FREM1 gene due to its known involvement in craniosynostosis. Two candidate variants were

identified in separate exons. The first variant is within exon 15 of RefSeq record NM_144966, causing a C2408A mutation. This corresponds to an S803W amino acid change. The second mutation is within exon 26 of RefSeq record NM_144966. This mutation is a G4504A change , corresponding to a V1502M amino acid change.

A list of all candidate genes identified, as well as the amount of variants left after each step is shown in Table 9 a and b. Detailed results from all families are shown in Appendix I.

Table 9a. Variants Left After Filtering Steps

	CS-58 (3 Generation)	CS-39 (*de novo* Trio)	CS-14 (MZ Twins)	CS-64 (Dominant Trio)	CS-2 (Recessive Family)
KGG and Excel Filtering	113	9	7	143	375
No rsID	29	-	-	40	-
SIFT < 0.5 and Polyphen_HDIV > 0.957	15	-	-	26	84
IGV Analysis	12	6	2	26	-
Functional Prediction	-	-	-	3	2

Table 9b. Candidate Genes for Each Family (* = Kept solely for sequencing)

CS-58	CS-39	CS-14	CS-64	CS-2
FGFR2	FGFR3	HRNR	ITGAV	FREM1 Ex15
		AR	SLC30A9	FREM1 Ex26
*			BAMBI	
MASP2				
PTPN7			*	
CCT4			CRELD1	
ANKMY7			SLC20A1	
TRDN				
CIZ1				
BHMT				
OR6T1				
TSPG1				
RNF157				
ZNF516				

Sanger Sequencing

Sequencing confirmed all variants within the CS-58 aside from ANKMY1, MASP2, and OR6T1. Successful primer sets to amplify these three genes were unable to be found and were not pursued. Sanger sequencing was also able to confirm the three CS-64 family variants and the FGFR3 mutation in the CS-39 family. Both variants within the CS-14 affected individual were shown to be unconfirmed. Within the six member CS-2 family, the mutation in FREM1 exon 15 was confirmed to be heterozygous in CS-2, CS-3, CS-5, homozygous alternate in CS-4, CS-6, CS-7. The FREM1 exon 26 mutation was confirmed to be homozygous reference in CS-2, homozygous alternate in CS-7, and heterozygous in all four of the children: CS-3, CS-4, CS-5, and CS-6.

A total of 70 samples were sent for Sanger Sequencing. This included 9 variants from the CS-58 family, 1 variant from the CS-39 trio, 5 variants from the CS-64 trio, 2 variants from the CS-14 twins, and 2 variants from the six member CS-2 family. Of these 70 samples, only the 2 from the affected CS-14 twin were shown to not be confirmed. The call made from Beckman Coulter Genomics, Inc. could have been wrong due to a low sequence quality or read depth.

CS-64 Candidate Gene Analysis

Once sequencing confirmed the three candidate mutations, each gene was analyzed in order to determine the effect of each mutation on the corresponding protein. The leucine to phenylalanine mutation in ITGAV occurs within a stretch of repeats called the “FG-GAP 1”. FG-GAP repeats are found in the N terminus of integrin alpha chains, a region that is important for ligand binding. The mutation is predicted to disrupt the repeat. Based upon conservation and amino acid properties, this mutation is predicted to be damaging to the protein, decreasing the stability.

The leucine to proline mutation in SLC30A9 is located within a stretch of amino acids annotated in the Uniprot database as a transmembrane domain. This transmembrane domain is predicted to be part of a zinc transporter. Because the mutant is smaller and more rigid than the wild-type residue, interactions between amino acids, as well as flexibility of the chain can be disrupted. Due to the possible disruption of the transmembrane function, this mutation is thought to be damaging to the protein and decrease the stability.

Not much is known about the methionine to valine mutation in BAMBI, except that it is located in a conserved domain. However, few other residues have been observed in the same position. Although valine is not one of these few, residues with similar properties have been observed in this position. This leads to the possibility that this mutation may increase the stability of the protein.

Functional Analysis of CS-64 Candidate Genes

After variants for the CS-64 family had been narrowed down through functional prediction and protein stability prediction, it was determined that two of the genes, ITGAV and SLC30A9 were candidate genes for knockdown studies. The other variant, BAMBI, was a candidate for overexpression studies. Knockdown studies were performed using a CRISPR/Cas9 method. The overexpression study was performed using a sub cloning method with a heat shock promoter vector.

At the 5-week time-point for the CRISPR/Cas9 injections, 5 of the zebrafish knockdown strains still had surviving individuals left out of the approximately 40 per line that were injected. All fish in the SLC30A9 Guide 2 knockdown line had died. Within the SLC30A9 Guide 1, 2 fish were surviving, so none were taken for staining at this 5 week time-point. The SLC30A9 Guide 3 line had 9 surviving fish, so 3 were taken for staining. Of the ITGAV lines, Guide 1 had 5 fish,

Guide 2 had 9 fish, and Guide 3 had 28 fish. Of these lines, 2 were taken for staining from the Guide 1 line, 3 were taken from the Guide 2 line, and 5 were taken from the Guide 3 line. There were 18 living control fish, so 3 were taken for staining. Results of the staining are shown in Figure 10. All fish within each gene group were similar in appearance, so a representative pictures is shown.

At the 8-week time-point for the CRISPR/Cas9 injections, 4 of the zebrafish knockdown strains still had surviving individuals. In addition to the previous expiration of the SLC30A9 Guide 2 knockdown fish, the SLC30A9 Guide 1 knockdown line had no surviving fish. The SLC309 Guide 3 strain had 6 surviving fish and all were taken for staining. Of the ITGAV knockdown lines, all 3 remaining fish from the Guide 1 line were taken, all 6 of the remaining fish of Guide 2 were taken, and 11 were taken from the surviving 23 of Guide 3. Of the control individuals, 5 were taken for staining. Staining results for the 8-week time-point are pending. Table 10 shows the amount of each strain left at each time point.

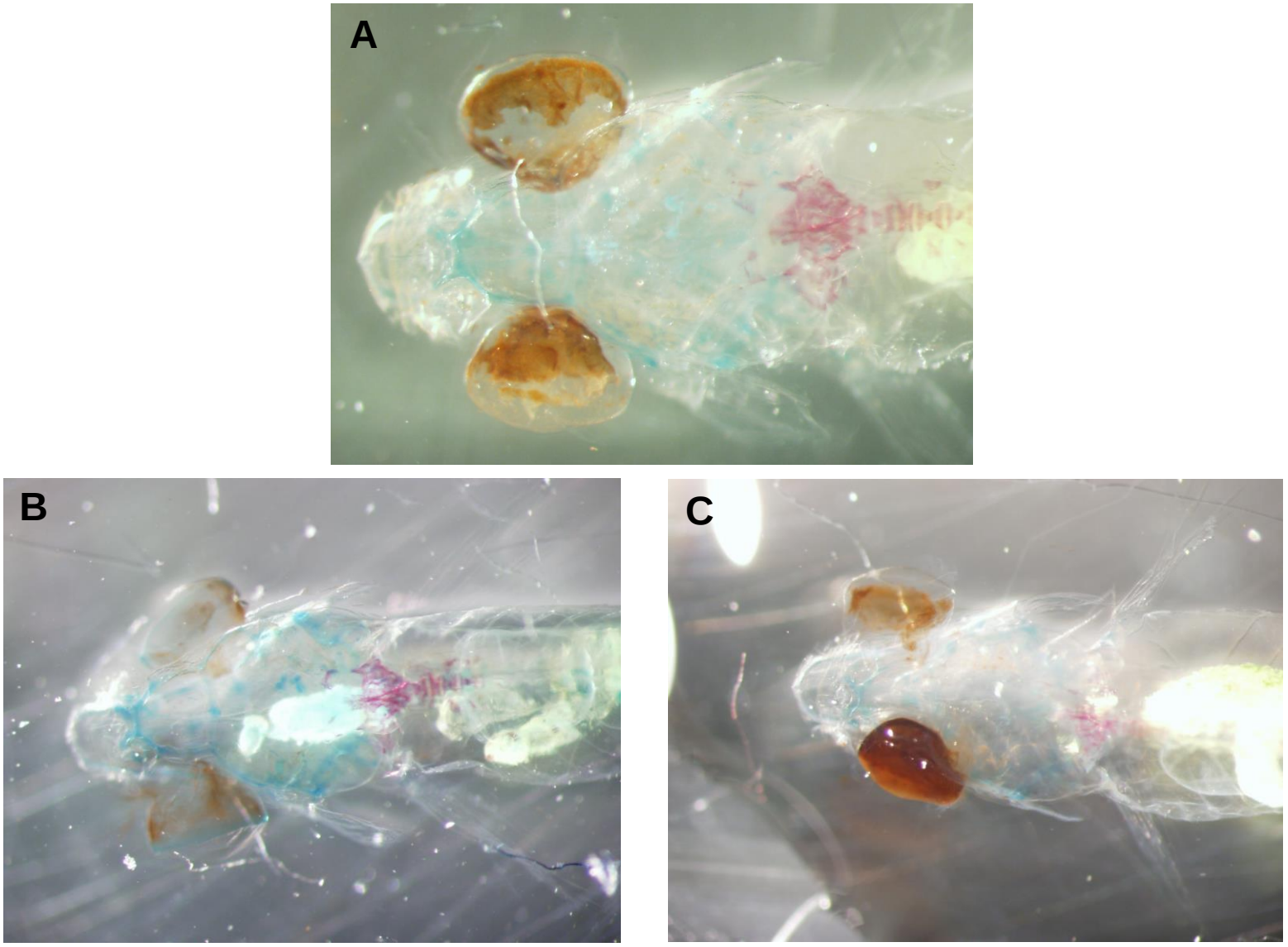

Figure 10. Staining results from 5-week time-point. Blue indicates cartilage and purple indicates bone. (A) Control fish. (B) ITGAV Guide 1 Knockdown. (C) SLC30A9 Guide 3 knockdown.

Table 10. Fish Left at Each Timepoint

	ITGAV Guide 1	ITGAV Guide 2	ITGAV Guide 3	SLC30A9 Guide 1	SLC30A9 Guide 2	SLC30A9 Guide 3	Control
Initially Injected	~40	~40	~40	~40	~40	~40	~80
Left at 5 weeks	5	9	28	2	0	9	38
Taken for staining at 5 weeks	2	3	5	0	0	3	3
Left after 5 week staining	3	6	24	2	0	6	35
Alive at 8 weeks	3	6	24	0	0	6	28
Taken for staining at 8 weeks	3	6	11	0	0	6	5

BAMBIa Cloning

Results for the BAMBIa overexpression are pending secondary to germline transmission.

Chapter 4: Discussion

It was of interest in this study to analyze both syndromic and nonsyndromic craniosynostosis patients in order to determine whether any candidate mutations could be identified. We had two syndromic families, one affected with Crouzon syndrome and one with Pfeiffer Type 3. Analysis of their exomes resulted in the identification of FGFR mutations, genes known to cause certain craniosynostosis syndromes. However, their phenotypes do not fit the reported phenotypes caused by their specific mutations, leading to an expansion for the phenotypical features caused by the mutation. The identification of several candidate genes in the nonsyndromic families opens up a direction for future research into the causes of NSC.

Mendelian Error Analysis

Although a significance difference was found when comparing the Mendelian errors of the proper family pedigree and the mean of the three simulations, there was still an excess amount of errors as compared with previous studies. Previous studies have shown an average of 3-5% of Mendelian errors found within a trio family (Patel, et al 2014 and O'Roak, et al 2012). Our variant findings make up approximately 6-7% of the sequence captured by sequencing. This can be explained, at least in part, by the method Beckman Coulter Genomics, Inc used for calling variants. They called variants beginning at the bases immediately following the primers as well as sequences adjacent but outside the exome capture areas. This can lead to a large amount of variants called due to low sequence quality at the areas directly flanking the primers. In addition, regions not part of, but adjacent to the capture regions have very low sequencing depth so calls are not accurate in these areas.

For the CS-14 twin pair, the small percentage of less than 0.001% of variants confirms the monozygotic nature of their relationship based upon comparison with previous studies (Chaiyasap, et al. 2014) (Peterson, et al, 2014).

Confirmation with Sanger Sequencing

Sanger Sequencing was able to confirm the correct variant calls in 68 out of the 70 samples sent for sequencing. The two unconfirmed sequences were the mutations expected in the CS-14 twin. These were both identified as heterozygous in CS-14 and homozygous for the reference allele in CS-15. However, upon Sanger Sequencing, the variants in CS-14 were shown to be homozygous for the reference allele. Reasons for this miscall could be that for the AR gene, there were only 13 reads total from CS-14, with 9 A (the reference allele) and 4 T (the mutant). For the HRNR variant, there as a deletion expected and it showed to be present in both twins. The CS-14 twin had 19 reads on this variant, and CS-15 had 22. Thus, the miscalls of these variants can be attributed to low sequence reads.

FGFR3 Mutations CS-39

The FGFR3 A391E mutation found in the CS-39 family has previously been studied in cases of Crouzon syndrome with AN. This mutation was of specific interest in FGFR3 studies because almost all documented FGFR3 mutations are associated with dwarfism syndromes of differing severities: achondroplasia (ACH, most common form of human dwarfish), Thanatophoric dysplasia (TD, lethal), and hypochondroplasia (HCH, mild). The primary difference between the mutations seen in most FGFR3 regions and the mutation associated with Crouzon with AN is the location of this mutation within the transmembrane region. Most FGFR3 mutations are found in the cytoplasmic tyrosine kinase domain, as well as in the third extracellular Ig-like domain (Figure 4). It has been shown that the A391E mutation stabilizes the

FGFR3 transmembrane domain homodimer in lipid bilayers, leading to over-stabilization of the FGFR3 dimers and increasing ligand-independent action. (Chen, et al. 2011).

Crouzon syndrome is an autosomal dominant disorder characterized by bicoronal synostosis, lip or cleft palate, midface hypoplasia, beaked nose, proptosis, and occasionally hearing loss. Hands and feet in individuals with Crouzon syndrome are typically structurally normal. AN is a skin disorder characterized by dark, thick, velvety skin in body folds and creases

CS-39 was born with complex synostosis involving the metopic, bicoronal, and lambdoid sutures. She also presented with proptosis, a tense and bulging fontanelle, midface hypoplasia, subsquamosal bulging, noisy breathing with gurgling, Chiari malformation, and turricephaly with a coned superior occiput and flattened lower occiput. In addition to her craniofacial abnormalities, she struggled with delayed gastric emptying, seizures, and kyphosis of her lower thoracic/upper lumbar spine. Genetic screening was performed in order to test for TWIST1 mutations, FGFR1 P252R mutation, FGFR3 P250R mutation, and sequencing of FGFR2 exons 3a, 3c, 8, and 10. The FGFR1 P252R mutation is a known cause of Pfeiffer syndrome and the FGFR3 P250R mutation is a known cause of Muenke syndrome. She was tested for the Muenke syndrome mutation due to the overlapping phenotypical features between the craniosynostosis syndromes. All results revealed no mutations. Clinically, CS-39 was classified as having Pfeiffer syndrome type 3, a syndrome that presents with complex synostosis, midface hypoplasia, hearing loss, severe proptosis, short anterior cranial base, and dental problems. Individuals with Pfeiffer syndrome also often have abnormalities in the hands and feet, such as syndactyly, bradydactyly, and an abnormally wide thumb and big toe that are bent away from other digits. Problems with the central nervous and gastrointestinal systems are common with these individuals (Hollier, 2015).

As shown in Figure 4, there is one mutation on FGFR1 that is known to cause Pfeiffer syndrome, and multiple mutations on FGFR2. However, no known mutations on FGFR3 have been known to cause Pfeiffer syndrome (Chen, et al). Identification of this mutation in an individual classified as having Pfeiffer syndrome leads to the possibility of variable expressivity. As shown in Figure 4, several mutations on FGFR2 lead to either Crouzon or Pfeiffer syndrome. These syndromes present with an overlapping phenotype, although Pfeiffer syndrome seems to present in a more severe manner. This increase in severity is primarily evidenced by the abnormalities often seen in the hands and feet, as well as increased suture fusions in Pfeiffer syndrome. The identification of this variant in CS-39, a case differing greatly from the classic phenotype of individuals with Crouzon with AN, can be possibly explained by the presence of another variant within either individuals with Crouzon with AN, or our individual. This other variant could be within a modifier gene that could cause the dysregulation of another protein within the pathway of the FGFR3 protein. Additionally, there could be reduced penetrance associated with this mutation, where a less severe form is the only phenotype that has been classified since its identification.

FGFR2 Mutation CS-58 Family

The FGFR2 mutation found in the three generation CS-58 family has previously been studied in one case of an individual with what was classified as Crouzon syndrome. Of all the known FGFR2 mutations within all disease types, 94% are found in exon 8, exon 10, or the intron sequence flanking exon 10. The Y105C mutation is found in exon 3 within the first Ig-like domain of the receptor and has been identified as the only known mutation within this domain (Kan, et al. 2002). This mutation creates a cysteine residue next to another cysteine at position

107, leading to the possibility of ligand-independent activation due to disulfide bonding (Yu, et al. 2000).

CS-58 presented with left coronal, left lambdoid, and squamous synostosis. He also had scalloping of the occipital bone and an unusually large anterior fontanelle. This patient had normal hearing, but low set ears. He showed no evidence of midface hypoplasia, but his palate was slightly arched and his left eye displayed ptosis with mild proptosis. This patient was diagnosed clinically as having atypical Crouzon based upon these findings and the absence of limb abnormalities. Prior to this study, genetic testing of CS-58 screened for FGFR3 mutations, with no mutations found.

Previously, the Y105C mutation has been identified in an individual with left coronal and sagittal synostosis, as well as moderate proptosis. This individual had normal limbs and digits, as well as normal development. Similar to CS-58, this patient was diagnosed with atypical Crouzon syndrome (Pulleyn, et al, 1997).

Although the Y105C mutation has only been seen a handful of times, leading to an inability to fully study the range of phenotypic features associated with it, we can assume that this mutation contributes to Crouzon syndrome, primarily in an atypical fashion. However, the identification of additional individuals with this mutation would help clarify its clinical implications.

FREM1 Mutations in CS-2 Family

Analysis of the two FREM1 mutations found in the six member CS-2 family revealed that the affected individuals (CS-3 and CS-4) have differing genotypes of the two variants. The affected individual CS-3 and unaffected individual CS-5 are both heterozygous for the variants in exon 15 and exon 26 and have the same genotype. Affected individual CS-4 and unaffected

individual CS-6 are both homozygous alternate for the variant in exon 15 and heterozygous for the variant in exon 26. Due to these findings, we can conclude that the FREM1 mutations are not likely, on their own, causative for the craniosynostosis phenotype found in this family. The FREM1 gene has been implicated in nonsyndromic metopic synostosis, but the two affected individuals in the CS-2 family are affected with sagittal synostosis. It is possible that the disease causing mutation is found within the exome sequencing that was performed, but further analysis is needed to narrow down candidate genes. There is also the possibility of the disease causing mutation being a combination of a FREM1 variant and another variant. Thus, further research into the FREM1 gene, as well as the results of the WES, is necessary to fully rule out this gene as causative for the craniosynostosis phenotype seen in CS-3 and CS-4.

CS-14 Twin Pair

Due to the lack of mutations found in the WES of the CS-14 twin family, it can be reasonably assumed that the disease causing mutation is within a segment of DNA that is missed by exome sequencing. WES misses approximately 15% of mutations. Mutations excluded by WES include those found in mitochondrial DNA, noncoding RNA, triplet repeat expansions, uniparental disomy, copy number variants, epigenetic changes, and intronic changes. Control sequences, or genes that control and modify other genes, are also often missed in WES because approximately half of the approximately 1,000 microRNAs are intronic (Belkadi, et al. 2015). Further research with this twin pair may involve WGS in order to identify the disease causing mutation. It is unlikely that environmental factors during the mother's pregnancy played a role, leaving a *de novo* genetic cause as the most likely reason for the discordance between the twins. The lack of identification of mutations within genes known to contribute to a craniosynostosis phenotype decreases the possibility of reduced penetrance. However, there could be a mutation

within a gene in both of the twins that has not yet been linked to craniosynostosis that presents with reduced penetrance, but this would require extensive testing on many different genes.

CS-64 Family Candidate Genes

Mutations known to cause nonsyndromic craniosynostosis have not yet been clearly identified. Of the few that are known, FGFR3 P250R has been associated with isolated coronal synostosis, as well as Muenke syndrome. FREM1mutations have been found in association with nonsyndromic metopic craniosynostosis. Sagittal synostosis, the most common type of craniosynostosis, has not yet had any causative mutations identified. CS-64 was born with nonsyndromic sagittal synostosis. CS-65, the father of CS-64, presented with clinical features indicative of sagittal synostosis. Thus, the identification of a candidate mutation within this family could lead to the possibility of further research into a cause of scaphocephaly. Three candidate genes were identified through KGGseq and Sanger sequencing as possible disease causing mutations for nonsyndromic sagittal synostosis. Mutations were found in genes ITGAV, SLC30A9, and BAMBI. These genes are discussed below.

ITGAV

Integrins serve as receptors for extracellular matrix-mediated cell adhesion, migration, cytoskeletal organization, cell proliferation, survival, and differentiation. Integrins function as heterodimers involving an alpha and beta subunit. They dimerize and bind with a ligand in order to communicate to the cell the character of extracellular matrix that is bound. There are 24 α subunits and 9 β subunits, but increased diversity is achieved by alternative splicing of the integrin RNA. Ligand binding with integrins is dependent on extracellular Ca^{2} or Mg^{2+}, depending on the integrin (Alberts, et al. 2002).

Interaction between an integrin and its ligand allows the cytoplasmic tail of the β subunit to bind a variety of intracellular anchor proteins, including talin, α-actinin, and filament. These anchor proteins can bind other anchor proteins such as actin or vinculin, thus linking the integrin to actin filaments in the cytoplasm. Signaling function depends on a cytoplasmic protein tyrosine kinase called the focal adhesion kinase (FAK). FAK is recruited to focal adhesions by talin, which binds to the β subunit; or paxillin, which binds to one type of α-integrin. Once multiple FAK molecules have clustered together, a phosphotyrosine docking site for members of the Src family of cytoplasmic tyrosine kinases is formed (Alberts, et al. 2002). Src then phosphorylates p130CAS and paxillin, which recruits the Crk-DOCK180 complex in order to activate Rac. Pac activates p21-activated kinase (PAK), Jun amino-terminal kinase (JNK), and nuclear factor κB (NF- κB). FAK can also activate extracellular signal-regulated kinase (ERK) and mitogen-activated protein kinase (MAPK) by recruiting RAP1. RAP1 activates ERK/MAPK through B-raf. FAK can also activate ERK/MAPK via growth factor bound 2 (GRB2) and son-of-sevenless (SOS) complex (Guo, et al. 2004) (Figure 11).

ITGAV encodes the α-5 subunit of the integrin family and has been implicated in many developmental processes. Alpha-5 has been shown to heterodimerize with β-1, 3, 5, 6, and 8. The α-5 subunit primarily interacts with the RGD sequence in a variety of ligands, including vitronectin, fibronectin, osteopontin, bone sialoprotein, thrombospondin, fibrinogen, von Willebrand factor, tenascin, and agrin. Integrin α5β8 is known to bind with laminin and type IV collagen (Hamosh, 2011). Previous knockout studies have shown that ablation of the gene for the α-5 integrin, although primarily causing lethality, allows considerable development and organogenesis, including extensive vasculogenesis and angiogenesis. From this trial, 20% of mice survived, but had considerable defects, including cleft palates, intracerebral hemorrhages,

and intestinal hemorrhages (Bader, et al 1998). Conditional knockout studies in mice have shown that α-5 integrins are central to intestinal immune regulation. Integrin α5β6 has been shown to associate with TGF- β1 in the skin and lungs. Knockout studies have shown that blocking TGF-β or its activation could be an effective treatment against pulmonary edema in acute lung injury (Lacy-Hubert, et al 2007).

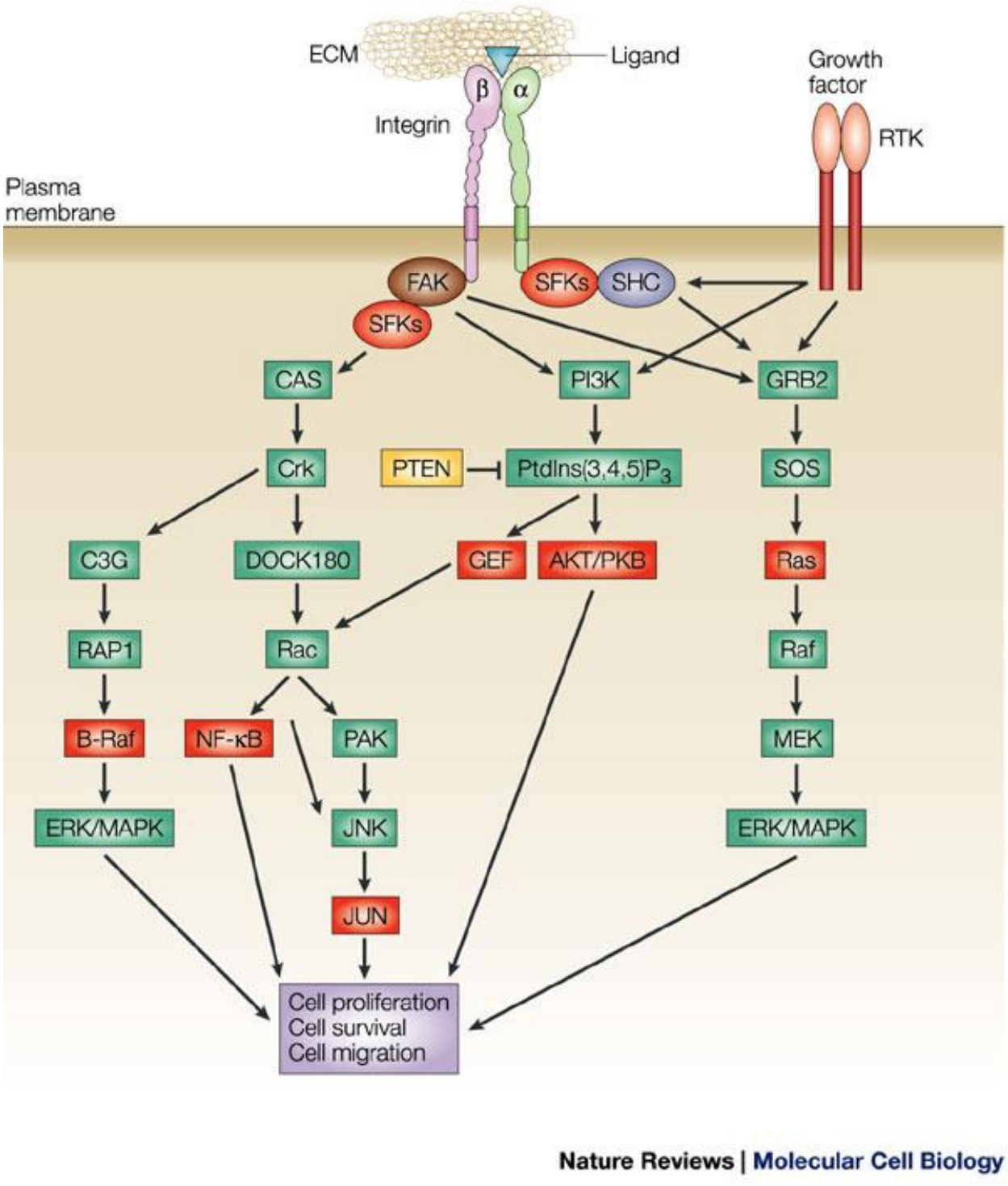

Figure 11. Integrin signaling pathway. Taken from Guo, et al. 2004

SLC30A9

SLC30A9 encodes member 9 from a family of several zinc transporters responsible for zinc homeostasis within the cell. Zinc is an essential element in organisms due to its function as a cofactor for hundreds of enzymes. Of the zinc transporter genes, SLC30 (ZnT) family genes are primarily responsible for facilitating removal of zinc from the cytosol, either out of the cell or into the lumen of vesicles or organelles. The SLC39 (ZIP) family of zinc transporters is responsible for the influx of zinc into the cytosol from either the outside of the cell or from the lumen of vesicles. These transporters are involved in several processes crucial to growth, development, reproduction, immunity, and bone formation (Cousins, et al. 2011).

Most members of the SLC30 family have 6 transmembrane domains and are predicted to have cytoplasmic amino and carboxy termini. Additionally, these proteins have a long histidine rich loop between transmembrane domains IV and V, the location where zinc is predicted to bind. With the exception of members 5 and 6, SLC30 members function as homodimers (Stephen, et al. 2012).

Inhibition of SLC30 family member 7 has shown increased osteogenic differentiation of mesenchymal stem cells. Overexpression of this same gene showed down regulation of beta-catenin. Beta-catenin is known to interact with Wnt genes in order to play a major role in the differentiation of mesenchymal stem cells. Another member of the zinc transporter family was shown to attenuate osteogenesis by inhibiting activated MAPK/ERK pathway, a signaling pathway known to play a role in differentiation of mesenchymal stem cells (Liu, et al. 2013). Not much is known about SLC30A9, but it was of significance for further analysis in our study due to noteworthy interactions of the SLC30 family members.

BAMBI

The BAMBI gene encodes a pseudo receptor for TGF-β that leads to inhibition of the TGF-β signaling pathway. TGF-β molecules cause downstream signaling through receptors that function as serine-threonine kinases to phosphorylate Smad proteins. Smad proteins then translocate to the nucleus to regulate TGF-β gene transcription (Figure 12). BAMBI exhibits structural homology to TGF-β receptor 1, but lacks the intracellular kinase domain. In lacking this domain, the BAMBI receptor acts as an antagonist to TGF superfamily members. (Luo, et al. 2012).

Not much is known about the physiological functions regulated by BAMBI, but it has been identified as a negative regulator of BMP during embryogenesis. However, studies have shown that knockouts of BAMBI show no phenotypic consequences during embryonic development. Mutant knockout mice were fertile, healthy, and displayed longevity that was comparable to wild-type littermates. BAMBI transcripts are abundantly seen in several CNS areas critical to pain processing, indicating a role for TGF-β in nociceptive regulation, both centrally and peripherally (Tramullas, et al. 2010). TGF-β is a multifunctional cytokine that controls proliferation, differentiation, migration, adhesion, and apoptosis of cells within the body. Blockage of TGF-β has been implicated in the progression of many carcinomas (Zhou, et al. 2013).

BAMBI proteins can also function as positive regulators of the Wnt/β-catenin pathway. Zhou et al. examined the role of BAMBI in osteosarcoma, a cancer of the bone, and found that its overexpression affected the intracellular expression of β-catenin, thus affecting the invasion and proliferation of osteosarcoma cells. A western blot showed that BAMBI expression was 4-fold higher in osteosarcoma tissues as compared to normal tissues. Cellular proliferation in a human osteosarcoma cell line was evaluated, revealing that BAMBI promoted the transition

from G0/G1 to G2/M in the cells. Collectively, this study showed that BAMBI modulated the Wnt/β-catenin pathway, suggesting that it can upregulate the invasion and migration of osteosarcoma cells. Additionally, BAMBI enhances cell viability by regulating the cell cycle in the presence of cyclin D1.

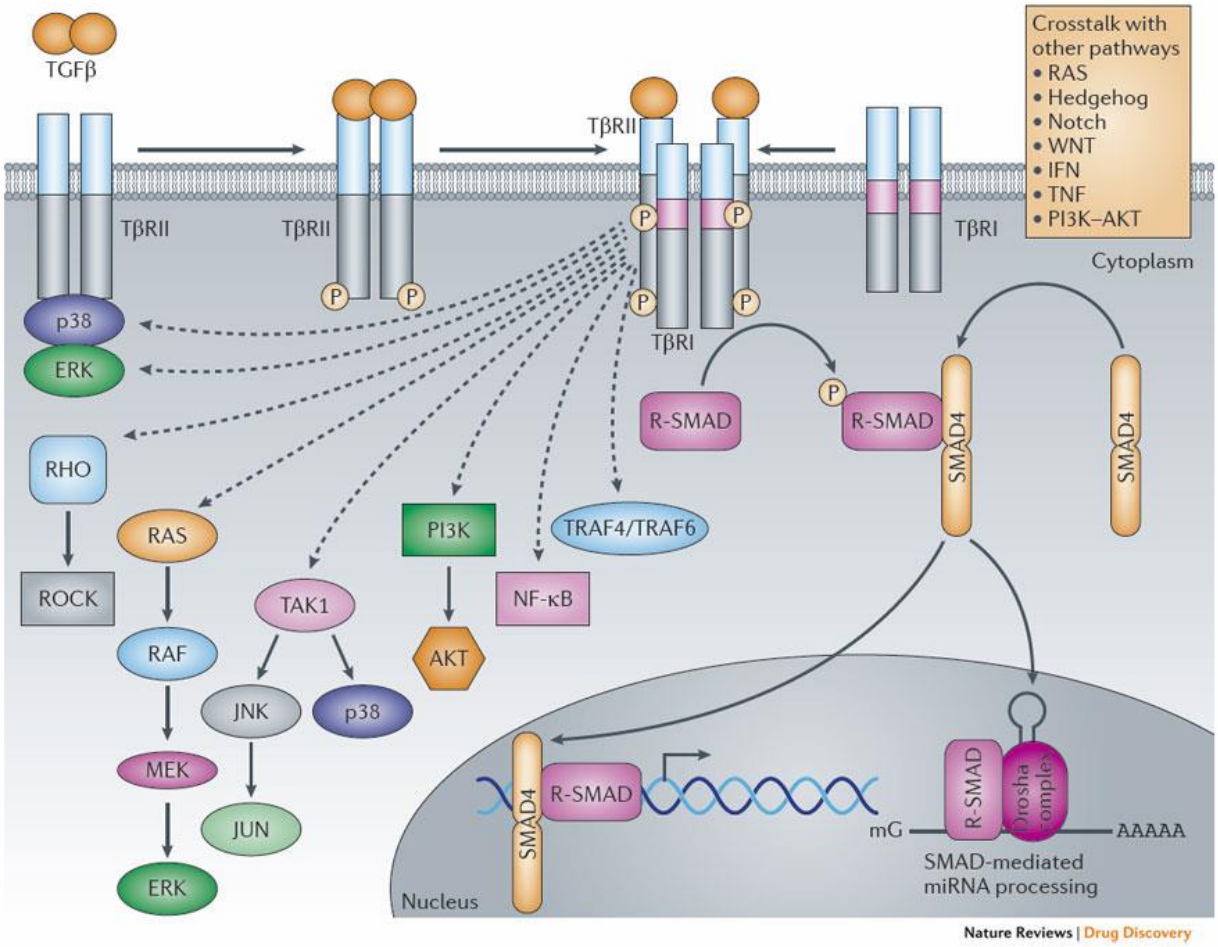

Figure 12. TGF-β R1 and R2 signaling. BAMBI exhibits similarity to TGF-β R1 signaling, but lacks the intracellular kinase domain.

Five Week Staining Results

It appears in the 5-week time point that there is more cartilage development in the ITGAV Guide 3 knockdown fish, whereas the SLC30A9 fish appears similar to the control. Without the genotyping of these fish, we are unable to draw a definitive conclusion about whether the increased cartilage in the ITGAV knockdown is caused by a mutation. Likewise, we are unable to conclude whether the SLC30A9 similarity in the control is caused by a mutation or lack of one. Thus, the 8-week staining and genotyping will provide further insight into whether the preliminary results with the 5-week staining is confirmed in further development.

The multiple deaths seen within both the SLC30A9 and the ITGAV knockdowns can be caused by several different factors. The injection process is often harsh on embryos and can cause skeletal abnormalities or even death. This is evidenced by the fact that many of the control embryos died, as well. Also, there is a possibility that the fish that died were positive for the knockout and it ended up killing them before analysis could be performed. Thus, it is necessary to perform further studies with these genes and inject another round of embryos for analysis and germline transmission.

BAMBI Overexpression

After functional analysis of the three candidate mutations within the CS-64 family, it is predicted that the disease causing mutation is found within the BAMBI gene. This hypothesis is primarily based upon the analysis of previous studies of BAMBI functions. It is predicted that the craniosynostosis phenotype is caused by an overexpression due to the lack of a phenotype shown in mouse knockout studies. Further investigation of the BAMBI gene requires generational analysis in zebrafish using the overexpression vector created within this study.

Future Studies

Future studies determining causes of nonsyndromic craniosynostosis will continue with the 100 samples that have been collected through the VCU Center for Craniofacial Care. We speculate that nonsyndromic craniosynostosis is a polygenic disorder, a disorder that can be caused by mutations in different genes. This prediction is supported by the identification of the candidate mutations within the CS-64 family compared with the lack of mutations found within the CS-14 family, where the affected individuals in both families presented with sagittal synostosis. Further sequencing and identification of candidate mutations with the individuals that we have collected DNA from will allow a better look into nonsyndromic craniosynostosis of all types.

For the BAMBI gene, we predict that overexpression studies in zebrafish will have an effect on skull suture formation. Generational studies will be performed in order to obtain homozygous mutants for the Bambia gene and evaluated the effect of the overexpression. As previously stated, zebrafish have two homologs of the BAMBI gene. Further analysis of the BAMBI would require testing with the Bambib gene in zebrafish. Analysis of the Bambi homologs has not yet been performed in order to determine whether both perform the same function or have slightly differing functions, thus indicating the need for this analysis. Further studies are needed for the ITGAV and SLC30A9 knockdown lines as well, in order to perform germline transmission analysis.

If overexpression analysis of BAMBI returns no significant findings, there is the possibility of a multigenic component to the individuals within the CS-64 family. In order to investigate this possibility, future studies can involve differing combination of ITGAV, SLC30A9, or BAMBI. Due to the prediction that SLC30A9 and ITGAV mutations decrease the stability of the protein, an overexpression of BAMBI with a knockdown of SLC30A9 or ITGAV

should be explored. In the event that no phenotype is found involving any combination of these three genes, WGS should be studied to determine whether there is a mutation within an intron or modifier gene causing the phenotype. As stated with the CS-14 family, WGS will allow a look at the 15% of mutations that can be missed in WES.

References

Alberts, B., Hohnson, A., & Lewis, J. (2002). Integrins. In *Molecular Biology of the Cell* (4th ed.). New York, New York: Garland Science.

Anantheswar Y N, Venkataramana N K. Pediatric craniofacial surgery for craniosynostosis: Our experience and current concepts: Part -1. Journal of Pediatric Neuroscience 2009; 4:86-99

Bader, B., Rayburn, H., Crowley, D., & Hynes, R. (1998). Extensive Vasculogenesis, Angiogenesis, and Organogenesis Precede Lethality in Mice Lacking All αv Integrins. *Cell, 95*(4), 507-519.

Beederman, M., Farina, E., & Reid, R. (2014). Molecular basis of cranial suture biology and disease: Osteoblastic and osteoclastic perspectives. *Genes & Diseases, 1*(1), 120-125.

Behrman RE, Jenson HB, Stanton BF, eds. Nelson Textbook of Pediatrics. 19th ed. Philadelphia, Pa: Saunders Elsevier; 2011:chap 585.12.

Belkadi, A., Bolze, A., Y, I., A, C., QB, V., A, A., & L, S. (2015). Whole-genome sequencing is more powerful than whole-exome sequencing for detecting exome variants. *Proceedings of the National Academy of Sciences*.

Carlo WA. Physical Examination of the Newborn Infant. In: Kliegman RM, Behrman RE, Jenson HB, Stanton BF, eds. Nelson Textbook of Pediatrics. 19th ed. Philadelphia, Pa: Saunders Elsevier; 2011:chap 88.2.

Chen, F., Degnin, C., Laederich, M., Horton, W., & Hristova, K. (2011). The A391E mutation enhances FGFR3 activation in the abscence of ligand. *Biochimica Et Biophysica Acta (BBA), 1808*(8), 2045-2050.

Chaiyasap, P., Kulawonganunchai, S., Srichomthong, C., Tongsima, S., Suphapeetiporn, K., Shotelersul, V., et al. (2014)., Whole genome and exome sequencing of monozygotic twins with trisomy 21, discordant for a congenital heart defect and epilepsy. *PLoS One. 9(6)*.

Ciurea, A., & Toader, C. (n.d.). Genetics of Craniosynostois. Retrieved from http://www.medandlife.ro/medandlife205.html

Cousins, R., Liuzzi, J., & Lichten, L. (2006). Mammalian Zinc Transport, Trafficking and Signals. *Journal of Biological Chemistry, 281*(34).

Derderian, C., & Seaward, J. (2012). Syndromic Craniosynostosis. *Seminars in Plastic Surgery, 26*(2), 64–75. doi:10.1055/s-0032-1320064

Dooley, K., & Zon, L. (2000). Zebrafish: A model system for the study of human disease. *Current Opinion in Genetics & Development, 10*(3), 252-256.

Garza, R. M., & Khosla, R. K. (2012). Nonsyndromic Craniosynostosis. *Seminars in Plastic Surgery*, *26*(2), 53–63. doi:10.1055/s-0032-1320063

Gilbert SF. Developmental Biology. 6th edition. Sunderland (MA): Sinauer Associates; 2000. Osteogenesis: The Development of Bones.

Greenwood, J., Flodman, P., Osann, K., Boyadjiev, S., & Kimonis, V. (2014). Familial incidence and associated symptoms in a population of individuals with nonsyndromic craniosynostosis. *Genetics in Medicine, 16*(4).

Gripp, K.W., McDonald-McGinn, D.M., Gaudenz, K., Whitaker, L.A., Bartlett, S.P., Glat, P., Cassileth, L., Mayro, R., Zackai, E., Muenke, M. (1998). Identification of a genetic cause for isolated unilateral coronal synostosis: a unique mutation in the fibroblast growth factor receptor 3. *Journal of Pediatrics 132(4),* 714-716.

Grova, M., Lo, D., Montoro, D., Hyun, J., Chung, M., Wan, D., & Longaker, M. (2012). Animal Models of Cranial Suture Biology. *Journal of Craniofacial Surgery, 7*(1), 1954-1958.

Guo, W., & Giancotti, F. (2004). Integrin signaling during tumor progression. *Nature Reviews Molecular Cell Biology, 5,* 816-826.

Hamosh, A. (2011, February 2). Integrin , Alpha-V; ITGAV. Retrieved from http://www.omim.org/entry/193210

Huelke, D. F. (1998). An Overview of Anatomical Considerations of Infants and Children in the Adult World of Automobile Safety Design. *Annual Proceedings / Association for the Advancement of Automotive Medicine*, *42*, 93–113.

Hughes, S. (1997). Differential expression of the fibroblast growth factor receptor (FGFR) multigene family in normal human adult tissues. *Journal of Histochemistry & Cytochemistry, 45*(7), 1005-1019.

Hollier, L. (2015, January 1). Craniosynostosis Syndromes. Retrieved from http://www.uptodate.com/contents/craniosynostosis-syndromes

Jiang, X., Iseki, R. Maxson, H.M. Sucov, G.M. Morris-Kay (2002) Tissues origins and interactions in the mammalian skull vault. Dev Biol 241:106-116.

Johnson, D., & Wilkie, A.O.M. (2011). Craniosynostosis. *European Journal of Human Genetics,* 19(4), 369-376. Doi:10.1038/ejhg.2010.235.

Kan, S., Elanko, N., Johnson, D., Cornejo-Roldan, L., Cook, J., Reich, E. W., … Wilkie, A. O. M. (2002). Genomic Screening of Fibroblast Growth-Factor Receptor 2 Reveals a Wide Spectrum of Mutations in Patients with Syndromic Craniosynostosis. *American Journal of Human Genetics*, *70*(2), 472–486.

Kimmel CB, Ballard WW, Kimmel SR, Ullmann B, Schilling TF (1995). Stages of embryonic development of the zebrafish. Dev Dyn. 1995 Jul;203(3):253-310.

Kinsman SL, Johnston MV. Craniosynostosis. In: Kliegman RM,
Lattanzi, W., Bukvic, N., Barba, M., Tamburrini, G., Bernardini, C., Michetti, F., & DiRocco, C. (2012). Genetic basis of single-suture synostoses: Genes, chromosomes, and clinical implications. *Child's Nervous System, 28*(9), 1301-1310.

Komori, T., Yagi, H., Nomura, S., Yamaguchi, A., Sasaki, K., et al. (1997). Targeted disruption of CBFA1 results in a complete lack of bone formation owing to maturational arrest of osteoblasts. *Cell, 89(5)* 755-764.

Lacy-Hulbert, A., Smith, A., Tissire, H., Barry, M., Crowley, D., Bronson, R., . . . Hynes, R. (2007). Ulcerative colitis and autoimmunity induced by loss of myeloid alphaV integrins. *PNAS, 104*(40).

Laue, K., Pogoda, H.-M., Daniel, P. B., van Haeringen, A., Alanay, Y., von Ameln, S., … Robertson, S. P. (2011). Craniosynostosis and Multiple Skeletal Anomalies in Humans and Zebrafish Result from a Defect in the Localized Degradation of Retinoic Acid. *American Journal of Human Genetics*, *89*(5), 595–606. doi:10.1016/j.ajhg.2011.09.015

Liu, Y., Yan, F., Yang, W., Lu, X., & Wang, W. (2013). Effects of zinc transporter on differentiation of bone marrow mesenchymal stem cells to osteoblasts. *Biological Trace Element Research, 154*(2), 234-43. doi:http://dx.doi.org/10.1007/s12011-013-9683-y

Luo, X., Hutley, L. J., Webster, J. A., Kim, Y.-H., Liu, D.-F., Newell, F. S., … Whitehead, J. P. (2012). Identification of BMP and Activin Membrane-Bound Inhibitor (BAMBI) as a Potent Negative Regulator of Adipogenesis and Modulator of Autocrine/Paracrine Adipogenic Factors. *Diabetes*, *61*(1), 124–136. doi:10.2337/db11-0998

Morriss-Kay, G. M., & Wilkie, A. O. (2005). Growth of the normal skull vault and its alteration in craniosynostosis: insights from human genetics and experimental studies. *Journal of Anatomy*, *207*(5), 637–653. doi:10.1111/j.1469-7580.2005.00475.x

Mundulos, S., Otto, F., Mundulos, C., Mulliken, JB., et al. (1997). Mutations involving the transcription factor CBFA1 cause cleidocranial dysplasia. *Cell*, *89(5).* 773-779.

Neilson, K.M., & Friesel, R.E. (1995). Constitutive activation of fibroblast growth factor receptor-2 by a point mutation associated with Crouzon syndrome. *Journal of Biology and Chemistry 270 (44)* 26037-26040

O'Niell, M., & McKusick, V. (2013, July 18). CRANIOSYNOSTOSIS 2; CRS2. Retrieved from http://www.omim.org/entry/604757

Otto, F., Thornell, AP., Crompton, T., Denzel, A., Gilmour, KC., et al. (1997). CBFA1, a candidate gene for cleidocranial dysplasia syndrome, is essential for osteoblast differentiation and bone development. *Cell, 89(5).* 765-771.

Qin, Q., Xu, Y., He, T., Qin, C., & Xu, J. (2012). Normal and disease-related biological functions of Twist1 and underlying molecular mechanisms. *Cell Research, 22*(1), 90-106.

O'Roak, B., Vives, L., Girirajan, S., Karakoc, E., Krumm, N., Coe, B., & Levy, R. (2012). Sporadic autism exomes reveal a highly interconnected protein network of de novo mutations. *Nature, 485*(7397), 246-250.

Patel, Z. H., Kottyan, L. C., Lazaro, S., Williams, M. S., Ledbetter, D. H., Tromp, hbGerard, … Kaufman, K. M. (2014). The struggle to find reliable results in exome sequencing data: filtering out Mendelian errors. *Frontiers in Genetics*, *5*, 16. doi:10.3389/fgene.2014.00016

Pavlakis, E., Chiotaki, R., Chalepakis, G., (2011). The role of Fras1/Frem proteins in the structure and function of basement membrane. *International Journal of Biochemistry and Cell Biology 43(4)* 987-995. Doi: 10.1016/j.biocel.2010.12.016.

Peterson, B.S., Spehlmann, M.E., Raedler, A., Stade, B., Thomsen., Rabionet, R., Rosenstiel, P., Schreiber, S., Franke, A. (2014). Whole genome and exome sequencing of monozygotic twins discordant for Crohn's disease. *BMC Genomics*. Doi:10.1186/1471-2164-15-564.

Pincus, D. (n.d.). Pediatric Craniosynostosis. Retrieved from http://neurosurgery.ufl.edu/patient-care/diseases-conditions/pediatric-craniosynostosis/

Pulleyn LJ, Reardon W, Wilkes D, Rutland P, Jones BM, Hayward R, Hall CM, Brueton L, Chun N, Lammer E, Malcolm S, Winter RM (1996) Spectrum of craniosynostosis phenotypes associated with novel mutations at the fibroblast growth factor receptor 2 locus. *European Journal of Human Genetics 4:283–291*

Potthoff, T. (1984). Clearing and staining techniques. In: Ontogeny and Systematics of Fishes (based on an international symposium dedicated to the memory of Elbert Halvor Ahlstrom). H.G. Moser, W.J. Richards, D.M. Cohen, M.P. Fahay, A.W. Kendall, Jr., and S.L. Richardson, eds. Lawrence, KS, Special Publication 1, American Society of Ichthyologists and Herpetologists, Allen Press, pgs. 35-37.

Quarto, N., & Longaker, M. (2005). The Zebrafish (Danio rerio): A model system for cranial suture patterning. *Cells Tissues Organs, 181*(2), 109-118.

Rabbani, B., Tekin, M., & Mahdieh, N. (2014). The promise of whole-exome sequencing in medical genetics. *Journal of Human Genetics, 59*(1), 5-15.

Rice, P. C., Rice, R., Thesleff, I. (2003), Molecular mechanisms in calvarial bone and suture development, and their relation to craniosynostosis. *European Journal of Orthodontics25(2),* 139-148.

Robin NH, Falk MJ, Haldeman-Englert CR. FGFR-Related Craniosynostosis Syndromes. 1998 Oct 20 [Updated 2011 Jun 7]. In: Pagon RA, Adam MP, Ardinger HH, et al., editors. GeneReviews® [Internet]. Seattle (WA): University of Washington, Seattle; 1993-2015. Available from: http://www.ncbi.nlm.nih.gov/books/NBK1455/

Stephen A. Myers, Alex Nield, and Mark Myers, "Zinc Transporters, Mechanisms of Action and Therapeutic Utility: Implications for Type 2 Diabetes Mellitus," Journal of Nutrition and Metabolism, vol. 2012, Article ID 173712, 13 pages, 2012. doi:10.1155/2012/173712

Talbot, J. C., & Amacher, S. L. (2014). A Streamlined CRISPR Pipeline to Reliably Generate Zebrafish Frameshifting Alleles. *Zebrafish*, *11*(6), 583–585. doi:10.1089/zeb.2014.1047

Thomas, G., Wilkie, A., Richards, P., Wall, S., (2005). FGFR3 P250R mutation increases the risk of reoperation in apparent 'nonsyndromic' coronal craniosynostosis. *Journal of Craniofacial Surgery 16(3),* 347-352.

Tramullas, M., Lantero, A., Diaz, A., Morchon, N., Merino, D., Villar, A., . . . Izpisua-Belmonte, J. (2010). BAMBI (bone morphogenic protein and activin membrane-bound inhibitor) reveals transforming growth factor beta family in pain modulation. *Journal of Neuroscience*, *30*(4).

Vissers, L. E. L. M., Cox, T. C., Maga, A. M., Short, K. M., Wiradjaja, F., Janssen, I. M., … Roscioli, T. (2011). Heterozygous Mutations of *FREM1* Are Associated with an Increased Risk of Isolated Metopic Craniosynostosis in Humans and Mice. *PLoS Genetics*, *7*(9), e1002278. doi:10.1371/journal.pgen.1002278

Yu, K., Herr, A. B., Waksman, G., & Ornitz, D. M. (2000). Loss of fibroblast growth factor receptor 2 ligand-binding specificity in Apert syndrome. *Proceedings of the National Academy of Sciences of the United States of America*, *97*(26), 14536–14541.

Zhou, L., Park, J., Jang, K., Park, H., Wagle, S., Yang, K., . . . Kim, J. (2013). The overexpression of BAMBI and its involvement in the growth and invasion of human osteosarcoma cells. *Oncology Reports*, *30*(3), 1315-1322.

Appendix

```
java -Xms256m -Xmx1300m
-jar ./kggseq/kggseq.jar
--buildver hg19
--resource ./resource
--no-resource-check
--no-lib-check
--out ./Trio1Rec
--excel
--vcf-file craSyn-Trio1.recode.vcf
--ped-file craSyn.ped
--genotype-filter 1,2,6
--seq-qual 30
--seq-mg 20
--seq-sb -10
--gty-qual 20
--gty-qual 8
--db-gene refgene
--gene-feature-in 0,1,2,3,4,5,6,7,8,9,10,11,12,13,14,15
--db-filter hg19_1kg201204,hg19_dbsnp138,hg19_ESP6500AA,hg19_ESP6500EA
--rare-allele-freq 0.01
--db-score dbnsfp
--mendel-causing-predict all
--genome-annot
--omim-annot
--candi-list
ALX4,BBS9,BMP2,BMP3,BMP4,BMP7,C1QTNF3,CYP26B1,EFNA4,ENFB1,MAPK1,ERK2,
ERK1,ERF,FAM20C,FBN1,FGF2,FGF7,FGF8,FGF9,FGFR1,FGFR2,FGFR3,FREM1,GLI3,GP
C3,IGF1R,IGF2R,IGFB3,IGFBP1,IGFBP5,IL11RA,KRAS,LMX1B,LRIT3,MCPH1,MSX2,NE
LL1,ORC1,POR,RAB23,RBP4,RECQL4,RUNX2,SFRP4,SKI,SNAI1,SOX6,TCF3,TCF12,TCO
F1,TGFB3,TGFBR1,TGFBR2,TWIST1,TWISTNB,WDR35,VCAM1,ZIC3
--ppi-annot-string
--ppi-depth 1
```

Appendix Ia. KGGseq script for CS-39 trio family. Recessive Filtering

```
java -Xms256m -Xmx1300m
-jar ./kggseq/kggseq.jar
--buildver hg19
--resource ./resource
--no-resource-check
--no-lib-check
--out ./Trio1Denovo
--excel
--vcf-file craSyn-Trio1.recode.vcf
--ped-file craSyn.ped
--genotype-filter 7
--seq-qual 30
--seq-mg 20
--seq-sb -10
--gty-qual 20
--gty-qual 8
--db-gene refgene
--gene-feature-in 0,1,2,3,4,5,6,7,8,9,10,11,12,13,14,15
--db-filter hg19_1kg201204,hg19_dbsnp138,hg19_ESP6500AA,hg19_ESP6500EA
--rare-allele-freq 0.01
--db-score dbnsfp
--mendel-causing-predict all
--genome-annot
--omim-annot
--candi-list
ALX4,BBS9,BMP2,BMP3,BMP4,BMP7,C1QTNF3,CYP26B1,EFNA4,ENFB1,MAPK1,ERK2,
ERK1,ERF,FAM20C,FBN1,FGF2,FGF7,FGF8,FGF9,FGFR1,FGFR2,FGFR3,FREM1,GLI3,GP
C3,IGF1R,IGF2R,IGFB3,IGFBP1,IGFBP5,IL11RA,KRAS,LMX1B,LRIT3,MCPH1,MSX2,NE
LL1,ORC1,POR,RAB23,RBP4,RECQL4,RUNX2,SFRP4,SKI,SNAI1,SOX6,TCF3,TCF12,TCO
F1,TGFB3,TGFBR1,TGFBR2,TWIST1,TWISTNB,WDR35,VCAM1,ZIC3
--ppi-annot-string
--ppi-depth 1
```

Appendix Ib. KGGseq script for CS-39 trio family. *De novo* filtering.

```
java -Xms256m -Xmx1300m
-jar ./kggseq/kggseq.jar
--buildver hg19
--resource ./resource
--no-resource-check
--no-lib-check
--out ./3Gen
--excel
--vcf-file craSyn-3Gen.recode.vcf
--ped-file craSyn.ped
--genotype-filter 3,4,5
--seq-qual 30
--seq-mg 20
--seq-sb -10
--gty-qual 20
--gty-qual 8
--db-gene refgene
--gene-feature-in 0,1,2,3,4,5,6,7,8,9,10,11,12,13,14,15
--db-filter hg19_1kg201204,hg19_dbsnp138,hg19_ESP6500AA,hg19_ESP6500EA
--rare-allele-freq 0.01
--db-score dbnsfp
--mendel-causing-predict all
--genome-annot
--omim-annot
--candi-list
ALX4,BBS9,BMP2,BMP3,BMP4,BMP7,C1QTNF3,CYP26B1,EFNA4,ENFB1,MAPK1,ERK2,
ERK1,ERF,FAM20C,FBN1,FGF2,FGF7,FGF8,FGF9,FGFR1,FGFR2,FGFR3,FREM1,GLI3,GP
C3,IGF1R,IGF2R,IGFB3,IGFBP1,IGFBP5,IL11RA,KRAS,LMX1B,LRIT3,MCPH1,MSX2,NE
LL1,ORC1,POR,RAB23,RBP4,RECQL4,RUNX2,SFRP4,SKI,SNAI1,SOX6,TCF3,TCF12,TCO
F1,TGFB3,TGFBR1,TGFBR2,TWIST1,TWISTNB,WDR35,VCAM1,ZIC3
--ppi-annot-string
--ppi-depth 1
```

Appendix Ic. KGGseq script for CS-58 three generation family. Dominant filtering.

```
java -Xms256m -Xmx1300m
-jar ./kggseq/kggseq.jar
--buildver hg19
--resource ./resource
--no-resource-check
--no-lib-check
--out ./Trio2
--excel
--vcf-file craSyn-Trio2.recode.vcf
--ped-file craSyn.ped
--genotype-filter 3,4,5
--seq-qual 30
--seq-mg 20
--seq-sb -10
--gty-qual 20
--gty-qual 8
--db-gene refgene
--gene-feature-in 0,1,2,3,4,5,6,7,8,9,10,11,12,13,14,15
--db-filter hg19_1kg201204,hg19_dbsnp138,hg19_ESP6500AA,hg19_ESP6500EA
--rare-allele-freq 0.005
--db-score dbnsfp
--mendel-causing-predict all
--genome-annot
--omim-annot
--candi-list
ALX4,BBS9,BMP2,BMP3,BMP4,BMP7,C1QTNF3,CYP26B1,EFNA4,ENFB1,MAPK1,ERK2,
ERK1,ERF,FAM20C,FBN1,FGF2,FGF7,FGF8,FGF9,FGFR1,FGFR2,FGFR3,FREM1,GLI3,GP
C3,IGF1R,IGF2R,IGFB3,IGFBP1,IGFBP5,IL11RA,KRAS,LMX1B,LRIT3,MCPH1,MSX2,NE
LL1,ORC1,POR,RAB23,RBP4,RECQL4,RUNX2,SFRP4,SKI,SNAI1,SOX6,TCF3,TCF12,TCO
F1,TGFB3,TGFBR1,TGFBR2,TWIST1,TWISTNB,WDR35,VCAM1,ZIC3
--ppi-annot-string
--ppi-depth 1
--pubmed-mining bone,skull,craniosynostosis,suture
```

Appendix Id. KGGseq script for CS-64 trio family. Dominant Filtering

```
java -Xms256m -Xmx1300m
-jar ./kggseq/kggseq.jar
--buildver hg19
--resource ./resource
--no-resource-check
--no-lib-check
--out ./MZ
--excel
--vcf-file craSyn-MZ.recode.vcf
--ped-file craSyn.ped
--genotype-filter 2,4
--seq-qual 30
--seq-mg 20
--seq-sb -10
--gty-qual 20
--gty-qual 8
--db-gene refgene
--gene-feature-in 0,1,2,3,4,5,6,7,8,9,10,11,12,13,14,15
--db-filter hg19_1kg201204,hg19_dbsnp138,hg19_ESP6500AA,hg19_ESP6500EA
--rare-allele-freq 0.01
--db-score dbnsfp
--mendel-causing-predict all
--genome-annot
--omim-annot
--candi-list
ALX4,BBS9,BMP2,BMP3,BMP4,BMP7,C1QTNF3,CYP26B1,EFNA4,ENFB1,MAPK1,ERK2,
ERK1,ERF,FAM20C,FBN1,FGF2,FGF7,FGF8,FGF9,FGFR1,FGFR2,FGFR3,FREM1,GLI3,GP
C3,IGF1R,IGF2R,IGFB3,IGFBP1,IGFBP5,IL11RA,KRAS,LMX1B,LRIT3,MCPH1,MSX2,NE
LL1,ORC1,POR,RAB23,RBP4,RECQL4,RUNX2,SFRP4,SKI,SNAI1,SOX6,TCF3,TCF12,TCO
F1,TGFB3,TGFBR1,TGFBR2,TWIST1,TWISTNB,WDR35,VCAM1,ZIC3
--ppi-annot-string
--ppi-depth 1
```

Appendix Ie. KGGseq script for CS-14 twin family.

A

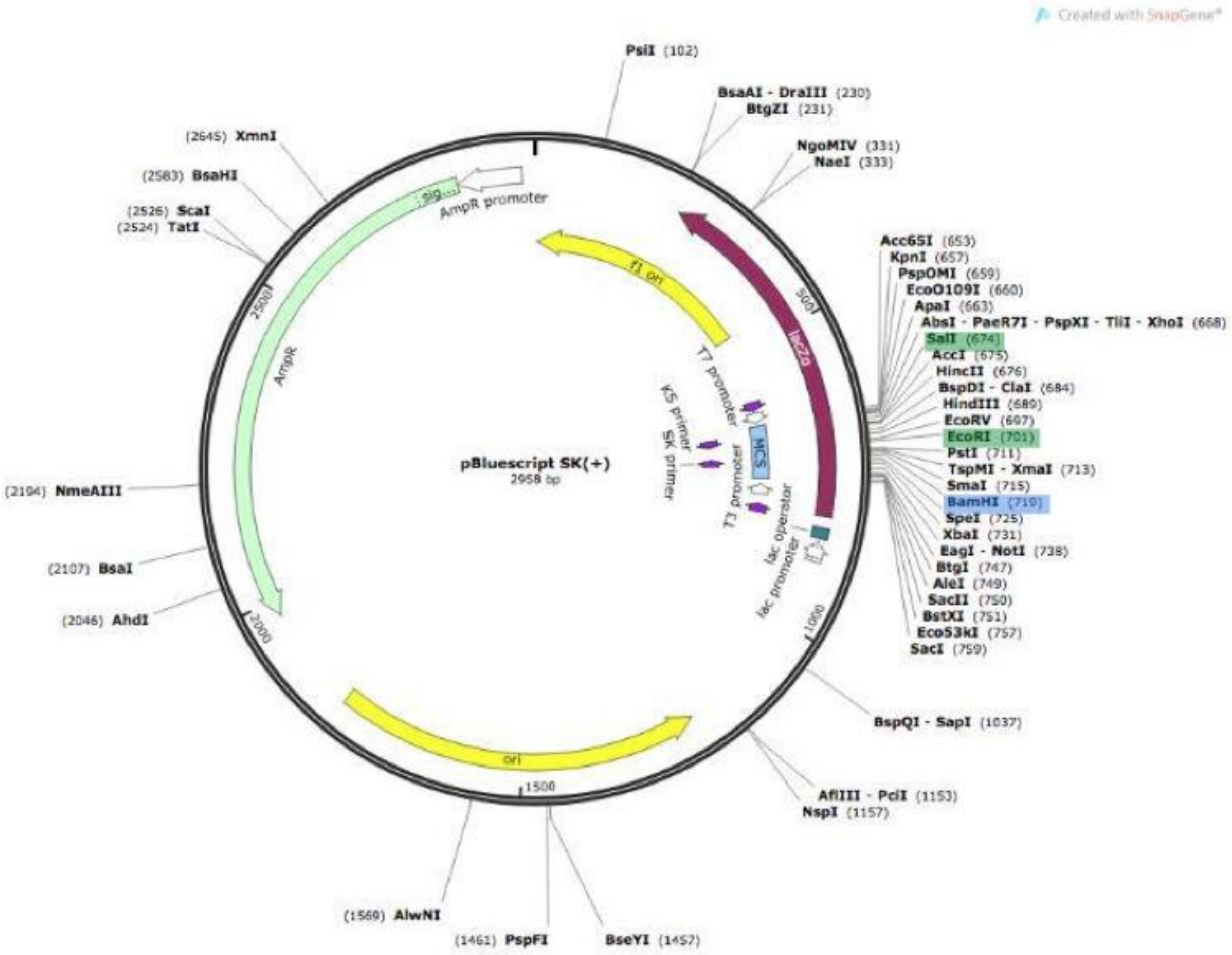

B

```
gcgtccggat cggggatagt tgcccttgtg gaaacttgtt tgtgttattt cacgagtccg
tttgcgtttt atatgtgttt gtgtgttttt catcgcatgg cggattggtt tggttacaca
cggggaatgt ttctccactc gcgctagttt cggatcctcc gatggaacaa gacgcgagcc
ttttctgcgc ccgtttgatt tttggataca gtgtagatca cagatccctg ggaatgcagt
aataaatgta ggacatatgt aacgagtcct ctcaaaccat tcggagggtc ttgccacggg
gtatcaagac aaggaaaagc agccgtaaat ggatcgcctg gtttctctgt ggtttcagct
ggaactttgt gcgatggctg ttcttctcac gaaaggagag atcaggtgct actgtgacgc
accgcactgc gttgccaccg gatacatgtg taaatcagag ctcaacgctt gctttactaa
ggtcctggac cctcttaaca caaactcacc tttaacacac ggctgcgtgg attcgctttt
aaactctgca gacgtgtgct ctagtaaaaa tgtggacatt tcaagtggaa gctcctctcc
tgtggagtgc tgccatgatg atatgtgtaa ctacaggggt ttgcatgacc tcacacaccc
cagaggggac tcaacagacc gataccacag ctccaatcag aacctgatca caagggtgca
agagttagcg tctgctaaag aggtgtggtt ccgggcggcg gtgatagcgg ttcccatcgc
gggtgggctt atcctggttc tgctgattat gctggcgttg cgaatgctcc gtagcgaaaa
caagcgtctc caggcacagc gccagcagat gctttctcgc ctgcattaca gctttcacgg
acaccaccat gccaagaaag gccacgtggc taagttggac ttggagtgta tggtgccggt
aacgggacat gagaactgtt gtctgggctg cgataagctg cggcagacgg atttgtgcac
tggaggagga agcgggggtg agcgtctcct atctctggta cactgggggа tgtacacggg
gcacggaaag ctggagttcg tatgactact cagagcttct ttgttagggc acaaaagggt
aactgtgtag tttgctgtcg taatgttatt attatcggcg tgttatttta ttgtctccaa
cgagagcaaa gacatttcaa ggacacaatt cattgtgttt tctcaaaaaa agagcacttt
acttgaatta gaatggccgg tctctgtggg gggctgtggt gaatatgaaa agggtggagc
ttatggactg caagccccac ctccttccct ctctggatcc tggaatgaca ctgaaggatt
cgttaagacg gtcttatttt gcacatttgt ataaaacgga cttgatgatt aaagttgtaa
ggtcgcagtc tgcgcccttt tttgaagaat tttacactga caccagggta cagataaggt
ttgttgtagt caaattgtat gaataaaaga ttcaatcttg actgtaaaaa aaaaaaaaaa
```

C

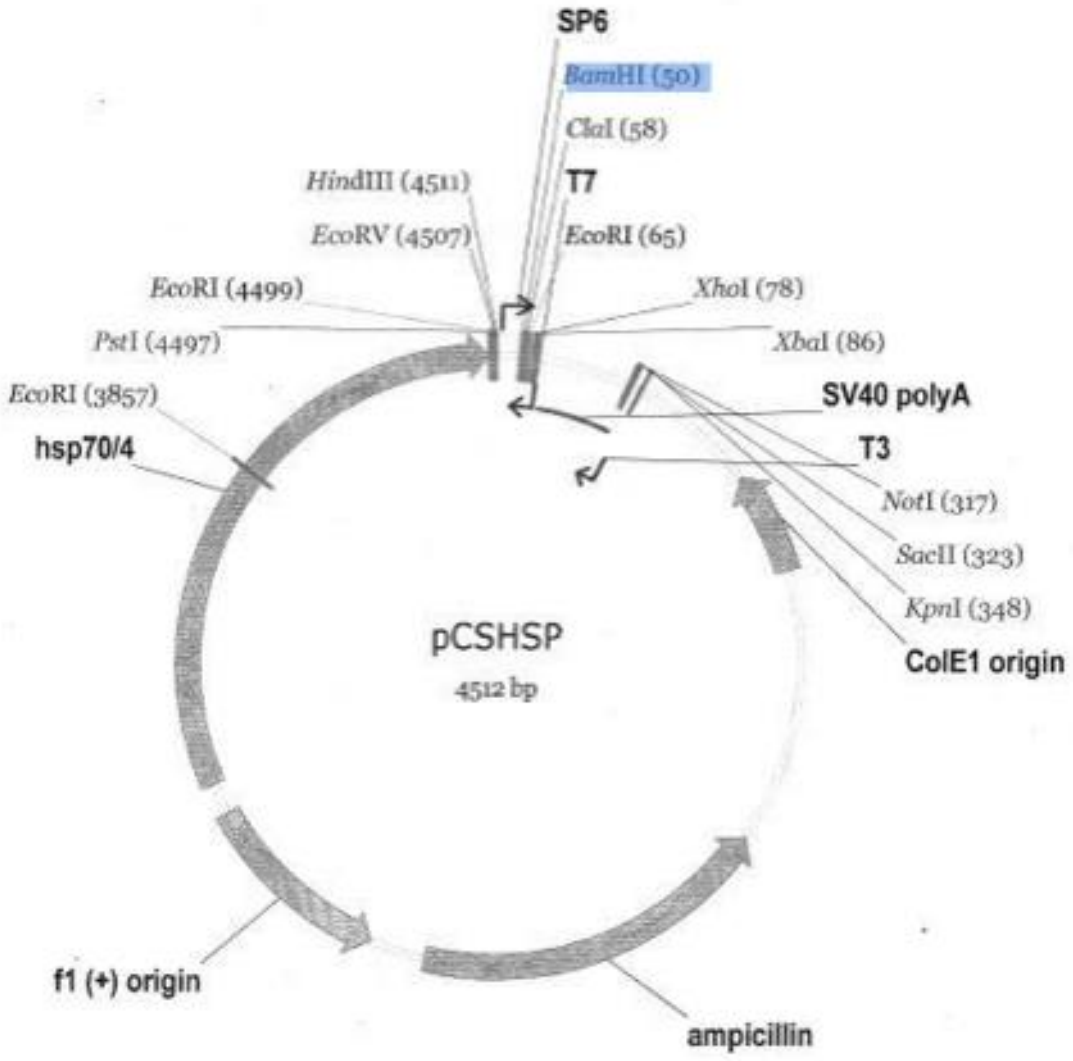

Appendix II. (A) A restriction site map of pBluescript SK- vector with green showing the location of the Bambia insert and the blue showing BamH1 cut sites (B) Bambia gene showing BamH1 cut sites in blue and coding DNA sequence in red. (C) pCSHSP heat shock promoter vector with blue showing BamH1 cut sites.

Chr	Position	Ref/Alt	rsID	Gene	Gene Feature	SIFT	Polyphen_HDIV	AffRef	AffHet	AffAlt	UnRef	UnHet	UnAlt
CS-39 Family: Affected Daughter CS-39 Unaffected Mother CS-54 Unaffected Father CS-55													
4	1806153	C/A	rs28931615	FGFR3	missense	0.059999999	0.921000004	0	1	0	2	0	0
CS-64 Family: Affected Daughter CS-64 Unaffected Mother CS-66 Affected Father CS-65													
2	187466761	C/T	.	ITGAV	missense	0	1	0	2	0	1	0	0
4	42068573	T/C	.	SLC30A9	missense	0.02	0.99599999	0	2	0	1	0	0
10	28971115	A/G	.	BAMBI	missense	0.300000012	0.96899998	0	2	0	1	0	0
CS-58 Family: Affected Son CS-58 Affected Mother CA-59 Unaffected Father CS-60 Affected Maternal Grandmother CS-61													
1	11107097	G/A	.	MASP2	missense	0.01	1	0	3	0	1	0	0
1	202129691	C/T	.	PTPN7	stopgain	0.49000001	.	0	3	0	1	0	0
2	62106135	T/C	.	CCT4	missense	0.029999999	0.964999974	0	3	0	1	0	0
2	241447012	C/T	.	ANKMY1	missense	0.02	0.998000026	0	3	0	1	0	0
5	78422030	G/A	.	BHMT	missense	0.07	1	0	3	0	1	0	0
6	123824803	A/G	.	TRDN	missense	.	.	0	3	0	1	0	0
9	130954172	C/T	.	CIZ1	missense	.	.	0	3	0	1	0	0
10	123325014	T/C	.	FGFR2	missense	0	1	0	3	0	1	0	0
11	123813831	A/T	.	OR6T1	missense	0	1	0	3	0	1	0	0
16	1272209	C/G	.	TPSG1	missense	0.159999996	0.961000025	0	3	0	1	0	0
17	74155468	G/A	.	RNF157	missense	0	0.999000013	0	3	0	1	0	0
18	74074460	C/G	.	ZNF516	missense	0	0.998000026	0	3	0	1	0	0
CS-14 Family: Proband CS-14 Unaffected twin: CS-15													
1	152195729	T/A	.	HRNR	missense	0	0.51800001	0	1	0	1	0	0
X	66765161	A/T	.	AR	missense	0.029999999	0.44800001	0	1	0	1	0	0
CS-2 Family: Unaffected Mother CS-2 Affected Daughter CS-3 Affected Son CS-4 Unaffected Son CS-5 Unaffected Daughter CS-6 Unaffected Father CS-7													
9	14776140	C/T	.	FREM1	missense	0.050000001	0.06	0	2	0	1	0	0
9	14819370	G/T	.	FREM1	missense	0	0.995	0	1	1	0	1	0

Appendix III

Gene	
CS-39 Family: Affected Daughter CS-39 Unaffected Mother CS-54 Unaffected Father CS-55	
FGFR3	FGFR3:NM_022965(16Exons):intronic7;FGFR3:NM_000142(18Exons):exon9:c.C1172A:p.A391E&missense;FGFR3:NM_001163213(18Exons):exon9:c.C1178A:p.A393E&missense
CS-64 Family: Affected Daughter CS-64 Unaffected Mother CS-66 Affected Father CS-65	
ITGAV	ITGAV:NM_001144999(30Exons):exon2:c.C61T:p.L21F&missense;ITGAV:NM_001145000(28Exons):exon2:c.C199T:p.L67F&missense;ITGAV:NM_002210(30Exons):exon2:c.C199T:p.L67F&missense
SLC30A9	SLC30A9:NM_006345(18Exons):exon13:c.T1079C:p.L360P&missense
BAMBI	BAMBI:NM_012342(3Exons):exon3:c.A568G:p.M190V&missense
CS-58 Family: Affected Son CS-58 Affected Mother CA-59 Unaffected Father CS-60 Affected Maternal Grandmother CS-61	
MASP2	MASP2:NM_139208(5Exons):exon2:c.C85T:p.R29C&missense;MASP2:NM_006610(11Exons):exon2:c.C85T:p.R29C&missense
PTPN7	PTPN7:NR_037663(10Exons):ncRNA;PTPN7:NR_037664(9Exons):ncRNA;PTPN7:NM_080588(9Exons):upstream-572;PTPN7:NM_001199797(10Exons):intronic1;PTPN7:NM_002832(10Exons):exon1:c.G245A:p.W82*&stopgain
CCT4	CCT4:NM_006430(14Exons):exon5:c.A391G:p.T131A&missense;CCT4:NM_001256721(13Exons):exon4:c.A301G:p.T101A&missense
ANKMY1	ANKMY1:NM_001282780(14Exons):intronic9;ANKMY1:NM_001282771(18Exons):exon13:c.G2491A:p.E831K&missense;ANKMY1:NM_001282781(17Exons):exon12:c.G1507A:p.E503K&missense;ANKMY1:NM_016552(17Exons):exon12:c.G2224A:p.E742K&missense;ANKMY1:NM_017844(14Exons):exon9:c.G1552A:p.E518K&missense
BHMT	BHMT:NM_001713(8Exons):exon6:c.G787A:p.D263N&missense
TRDN	TRDN:NM_001256020(9Exons):intronic8;TRDN:NM_001251987(21Exons):intronic8;TRDN:NM_006073(41Exons):intronic8;TRDN:NM_001256021(8Exons):exon8:c.T854C:p.M285T&missense
CIZ1	CIZ1:NM_001131016(17Exons):upstream-304;CIZ1:NM_001131018(17Exons):upstream-304;CIZ1:NM_001131017(18Exons):upstream-304;CIZ1:NM_001257976(16Exons):upstream-304;CIZ1:NM_012127(17Exons):intronic1;CIZ1:NM_001131015(18Exons):intronic1;CIZ1:NM_001257975(18Exons):exon1:c.G47A:p.R16Q&missense
FGFR2	FGFR2:NR_073009(17Exons):ncRNA;FGFR2:NM_001144919(17Exons):intronic2;FGFR2:NM_001144918(16Exons):intronic2;FGFR2:NM_001144915(17Exons):intronic2;FGFR2:NM_001144916(15Exons):intronic1;FGFR2:NM_023029(16Exons):intronic1;FGFR2:NM_001144913(17Exons):exon2:c.A314G:p.Y105C&missense;FGFR2:NM_000141(18Exons):exon3:c.A314G:p.Y105C&missense;FGFR2:NM_022970(18Exons):exon3:c.A314G:p.Y105C&missense;FGFR2:NM_001144917(16Exons):exon3:c.A314G:p.Y105C&missense;FGFR2:NM_001144914(15Exons):exon2:c.A314G:p.Y105C&missense
OR6T1	FGFR3:NM_022965(16Exons):intronic7;FGFR3:NM_000142(18Exons):exon9:c.C1172A:p.A391E&missense;FGFR3:NM_001163213(18Exons):exon9:c.C1178A:p.A393E&missense
TPSG1	CACNA1H:NM_001005407(34Exons):downstream+437;CACNA1H:NM_021098(35Exons):downstream+437;TPSG1:NM_012467(6Exons):exon5:c.G644C:p.G215A&missense
RNF157	RNF157:NM_052916(19Exons):exon12:c.C1252T:p.R418C&missense
ZNF516	ZNF516:NM_014643(8Exons):exon8:c.G3485C:p.G1162A&missense
CS-14 Family: Proband CS-14 Unaffected twin: CS-15	
HRNR	HRNR:NM_001009931(3Exons):exon2:c.A1T:p.M1L&missense
AR	AR:NM_000044(8Exons):exon1:c.A173T:p.Q58L&missense
CS-2 Family: Unaffected Mother CS-2 Affected Daughter CS-3 Affected Son CS-4 Unaffected Son CS-5 Unaffected Daughter CS-6 Unaffected Father CS-7	
FREM1	.:FREM1:NM_144966(38Exons):exon26:c.G4504A:p.V1502M&missense;FREM1:NM_001177704(14Exons):exon2:c.G112A:p.V38M&missense
FREM1	.:FREM1:NM_144966(38Exons):exon15:c.C2408A:p.S803Y&missense

Appendix IV